Optics and Lasers in Engineering **19** (1993) 3–41

Application of Coherent Gradient Sensing (CGS) to the Investigation of Dynamic Fracture Problems

A. J. Rosakis

Graduate Aeronautical Laboratories, Division of Engineering and Applied Sciences, California Institute of Technology, Pasadena, California 91125, USA

ABSTRACT

In this paper we review recent theoretical and experimental developments related to the investigation of dynamic and transient crack-tip deformations using a new coherent optical technique—coherent gradient sensing (CGS). CGS is a full-field, lateral-shearing interferometric technique with an on-line spatial filter. This full-field optical method has been used both in transmission and reflection modes to study deformations in transparent as well as opaque solids. Its ability to produce fringes in real time is used advantageously to map dynamic crack-tip deformations in PMMA and AISI-4340 steel specimens as well as in bimaterial combinations of PMMA/Al and PMMA/steel. The technique measures either in-plane stress gradients (transmission) or out-of-plane displacement gradients (reflection).

INTRODUCTION

In experimental fracture studies, coherent gradient sensing (CGS),[1,2] photoelasticy,[3,4] caustics,[5] geometric moiré[6] and moiré interferometry[7] are some of the methods used to measure crack-tip deformations or deformation-related quantities and hence the stress-intensity factor. In these techniques, interpretation of the measurements is based on the premise that a K-dominant or a J-dominant two dimensional asymptotic field description exists in the vicinity of the crack tip. However, in reality, the situation has not been that simple. Recent studies[8–11] have

Optics and Lasers in Engineering 0143-8166/93/$06·00

brought to light the shortcomings of such interpretations because of the three-dimensional nature of the crack-tip deformation and the inadequacy of the purely singular fields to model the region outside the three-dimensional zone (lack of K- or J-dominance).

From these experimental and analytical investigations,[8–11] it has become increasingly evident that a two-dimensional K-dominant crack-tip field description for general specimen configurations should be used cautiously, keeping in mind the near-tip three dimensionality and possible lack of K-dominance. Furthermore, in dynamic loading situations, these complexities are compounded by the transient nature of the fracture phenomenon which may inhibit the establishment of a K_I^d-dominant region.[9,10] In view of the above, besides demonstrating the applicability of CGS to dynamic fracture studies, we will also examine some aspects related to lack of K_I^d-dominance.

Since CGS fringes are related to either in-plane stress gradients (transmission) or out-of-plane displacement gradients (reflection), the technique can be thought of as the *full field* equivalent of the optical method of caustics (for both the transmission and reflection cases). The sensitivity of the method to the same deformation or stress quantities responsible for the formation of caustics provides a unique opportunity for comparison. In particular, for transient dynamic fracture studies where the accurate interpretation of caustics has been questioned,[9,12] dynamic CGS has allowed for the direct investigation of the causes that lead to problems with caustics. In addition, the capability of CGS to investigate dynamic fracture problems in opaque materials (no severe light limitations resulting from exposure times of the order of nanoseconds) make this full-field technique a strong contender to caustics. Caustics by reflection have so far been the dominant optical method applied to the study of dynamic crack growth problems in *opaque* structural materials.[5,13,14]

Finally, in the last part of this paper we describe the initial steps of an investigation aimed towards the understanding of the mechanics of dynamic initiation and dynamic crack growth in interfaces between materials characterized by high mechanical property mismatch.

THE PHYSICAL PRINCIPLE OF CGS

Consider a planar wave front normally incident on an optically and mechanically isotropic, transparent plate of initial uniform thickness h

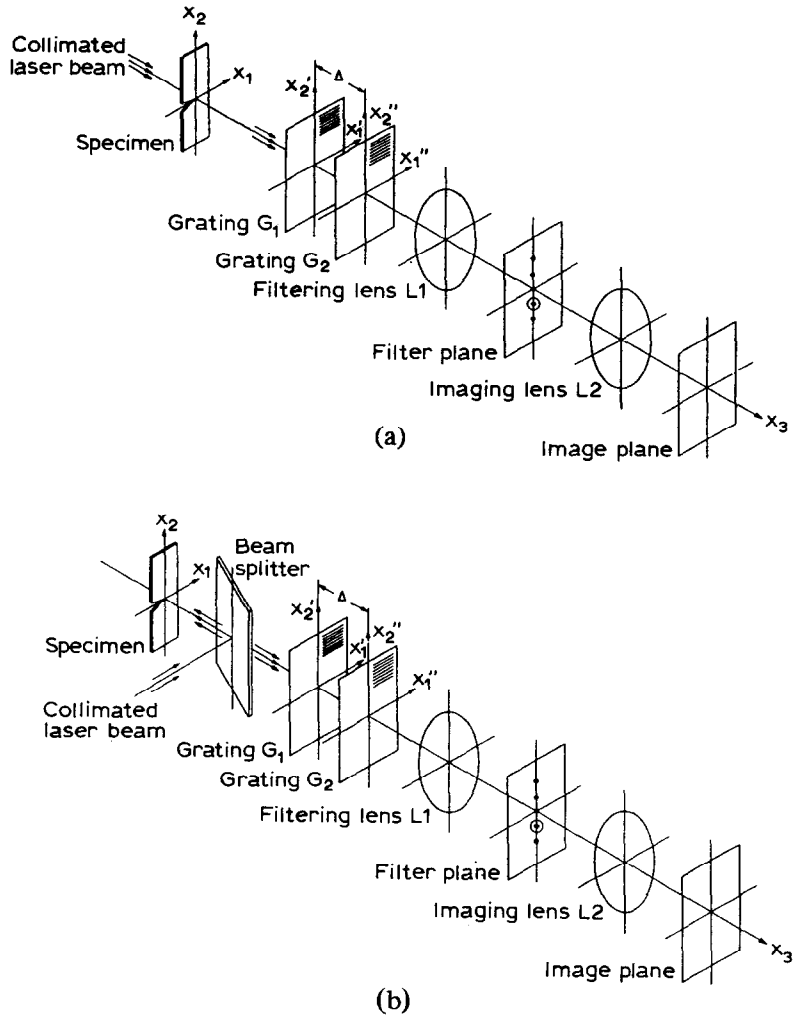

Fig. 1. Schematic representation of the experimental set-up for (a) transmission CGS and (b) reflection CGS.

and refractive index n. The specimen occupies the (x_1, x_2) plane in the undeformed configuration (Fig. 1). If the plate is deformed, the transmitted wave front will be expressed as $S(x_1, x_2, x_3) = x_3 + \Delta S(x_1, x_2) = \text{const.}$, where ΔS is the optical path change acquired during refraction. As discussed in detail by Rosakis,[5] ΔS is related to the deformation state by the relation

$$\Delta S(x_1, x_2) = 2h(n-1)\int_0^{1/2} \varepsilon_{33} d(x_3/h) + 2h\int_0^{1/2} \Delta n d(x_3/h) \qquad (1)$$

The first term of eqn (1) represents the net optical path difference due to the plate thickness change caused by the strain component ε_{33}. The second term is due to the stress-induced change in refractive index of the material. This change in the refractive index Δn is given by the Maxwell relation:[13]

$$\Delta n = D_1(\sigma_{11} + \sigma_{22} + \sigma_{33})$$

where D_1 is the stress optic constant and σ_{ij} are Cartesian components of the stress tensor. The above relation is stricly true for isotropic linear elastic solids. For such solids the strain component ε_{33} can also be related to the stresses and eqn (1) becomes:[5]

$$\Delta S(x_1, x_2) = 2hc_\sigma \int_0^{1/2} \left\{(\sigma_{11} + \sigma_{22})\left[1 - D_2\left(\frac{\sigma_{33}}{\nu(\sigma_{11} + \sigma_{22})}\right)\right]\right\} d(x_3/h) \quad (2)$$

where

$$c_\sigma = \left[D_1 - \frac{\nu}{E}(n-1)\right]$$

$$D_2 = -\left[\frac{\nu D_1 + \dfrac{\nu(n-1)}{E}}{D_1 \dfrac{\nu(n-1)}{E}}\right]$$

E, ν and c_σ are the Young's modulus, the Poisson's ratio and the stress optical coefficient of the material, respectively.

The CGS set-up described below is sensitive to in-plane gradients of optical path changes $\Delta S(x_1, x_2)$. For CGS by reflection, an equivalent relation for ΔS is obtained. The optical path difference in this case is associated with non-uniform surface elevations of an initially flat undeformed specimen surface. For this case, $\Delta S = 2u_3$, where u_3 is the out-of-plane displacement on the specimen surface. For a linear elastic solid ΔS is still given by eqn (2), with $c_\sigma = -\nu/E$ and $D_2 = 1$ (see Rosakis[5]).

THE EXPERIMENTAL SET-UP

The schematic of the transmission and reflection experimental arrangements are shown in Fig. 1(a) and (b). When the transmitted or reflected wave front emerges from the specimen after refraction or reflection, it

is processed by a pair of high-density gratings, G_1 and G_2, separated by a distance Δ. In a typical set-up, the gratings have their rulings parallel to either the x_1- or the x_2-axis. The grating pitch is denoted by p.

The light field emerging from G_2 is collected by the filtering lens L_1 and its frequency content (diffraction spots) is displayed on its back focal plane. By locating a filtering aperture around either ± 1 diffraction orders, information regarding the gradients components of $\Delta S(x_1, x_2)$ along either the x_1- or x_2-axis is obtained on the image plane. The camera consisting of the lens L_1 and image plane, is kept focused on the object plane. For gratings rulings perpendicular to the x_α-axis the resulting fringe pattern are proportional to $\partial(\Delta S)/\partial x_\alpha$, $\alpha = (1, 2)$.

More specifically, and as demonstrated by a first-order analysis described by Tippur *et al.*,[2] the resulting fringes can be related to gradients of $\Delta S(x_1, x_2)$ as follows:

$$\frac{\partial(\Delta S)}{\partial x_\alpha} = \frac{k_\alpha p}{\Delta}, \qquad \alpha = (1, 2) \tag{3}$$

where

$$k_\alpha = \begin{Bmatrix} m \text{ for } \alpha = 1,\ m = 0,\ \pm 1,\ \pm 2, \ldots \\ n \text{ for } \alpha = 2,\ n = 0,\ \pm 1,\ \pm 2, \ldots \end{Bmatrix}$$

and m and n are the fringe orders for the x_1 and x_2 gradient countours, respectively.

INFLUENCE OF THREE-DIMENSIONALITY ON DATA ANALYSIS

The discussion of the previous section was intentionally kept as general as possible within the assumptions of isotropic linear elasticity. For either a homogeneous or a bimaterial cracked linear elastic plate of uniform thickness and finite in-plane dimensions, the optical path difference ΔS in general will depend on the details of the three-dimensional elastostatic or elastodynamic stress state that would exist at the vicinity of the crack tip. This will be a function of the applied loading and the in-plane dimensions and thickness of the specimen as well as on the material properties mismatch in the case of bimaterials.

Given the lack of full-field, three-dimensional analytical solutions in fracture mechanics, experimental information can strictly be extracted

by means of detailed numerical calculations. Nevertheless, there exist certain non-trivial special cases for which available asymptotic solutions, based on two-dimensional analyses, may provide adequate approximations for $\Delta S(x_1, x_2)$ at certain regions near the crack tip. In particular, it has been argued that conditions of *plane stress* will dominate in thin, *homogeneous* cracked plates at distances from the crack front larger than half the specimen thickness. This would imply that if only fringes outside the three-dimensional zone are analyzed the results could be interpreted on the basis of a plane stress analysis.[5–11,13]

To visually illustrate the extend of the near-tip three-dimensionality, reference is made to Fig. 2, which shows a three-dimensional representation of the ratio $\sigma_{33}/\nu(\sigma_{11} + \sigma_{22})$ for a three-point bend specimen of a linear elastic, homogeneous material. It should be noted that this ratio appears in the second term of the intergrand of the optical path difference relation eqn (2). The ratio is often called the degree of plane strain. This ratio is a measure of near-tip three-dimensionality and is obtained by means of three-dimensional finite element calculation which models a stationary crack in a three-point bend specimen subjected to dynamic loading. In regions where the deformation is locally plane stress, this measure is equal to zero. When the deformation approaches the plane strain-like condition the ratio approaches the value of 1. In the figure, only one-half of the specimen thickness is shown. The top surface corresponds to the mid-plane of the specimen. The traction-free crack face is on the left-hand side of the picture. The maximum extent of the three-dimensional zone is approximately $0{\cdot}4$–$0{\cdot}5h$, $(\theta = 0)$, whereas at approximately $\theta \approx 120°$, the plane stress approximation is adequate very close to the crack tip $r \sim 0{\cdot}1h$.[5]

For points outside the three-dimensional region, a plane stress approximation will be applicable $(\sigma_{33}/\nu(\sigma_{11} + \sigma_{22}) \to 0)$. Indeed, for such points, the optical path difference ΔS (eqn (2)), which involves the ratio $\sigma_{33}/\nu(\sigma_{11} + \sigma_{22})$, will simplify to

$$\Delta S(x_1, x_2) \approx c_\sigma h[\hat{\sigma}_{11}(x_1, x_2) + \hat{\sigma}_{22}(x_1, x_2)] \tag{4}$$

where $c_\sigma = (D_1 - (\nu/E)(n-1))$ and $\hat{\sigma}_{11}$ and $\hat{\sigma}_{22}$ are *thickness averages* of the stress components in the plate. In the above expression c_σ is called the stress optical coefficient.

Indeed, for points outside the near-tip three-dimensional zone the CGS patterns assume a simple interpretation in terms of two-dimensional stress field approximations. In particular, eqns (3) and (4) now indicate that the fringes obtained from regions surrounding the three-dimensional zones can be related to the in-plane gradients of

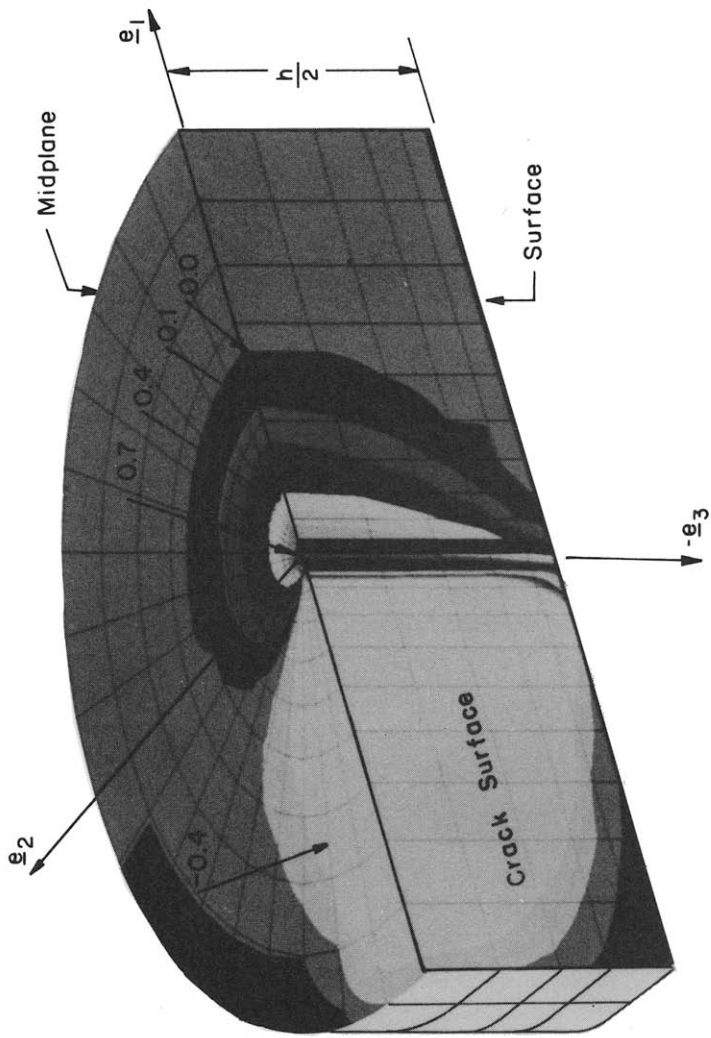

Fig. 2. Plane strain constraint near a through-thickness crack in a homogeneous elastic plate of uniform thickness h. Only half of the plate thickness is shown. The top surface is the mid-plane of the specimen.

$\hat{\sigma}_{11} + \hat{\sigma}_{22}$ as follows:

$$c_\sigma h \frac{\partial(\hat{\sigma}_{11} + \hat{\sigma}_{22})}{\partial x_2} = \frac{mp}{\Delta} \tag{5}$$

or

$$c_\sigma h \frac{\partial(\hat{\sigma}_{11} + \hat{\sigma}_{22})}{\partial x_1} = \frac{np}{\Delta}$$

In practical applications of the technique, only fringes outside the three-dimensional zone should be analyzed, since this is a *variable sensitivity* method (for fixed p, sensitivity is increased if the spacing between gratings, Δ, is increased); this can be achieved by choosing a ratio Δ/p such that enough experimental data are obtained outside the near-tip three-dimensional zone ($r \geq 0{\cdot}5h$).

If the plane stress region surrounding the near-tip three-dimensional zone is well described by the asymptotic expression for the stresses (conditions of K-dominance) then relations (5) can be used to estimate fracture parameters.

DYNAMIC CRACK GROWTH IN HOMOGENEOUS SOLIDS

Consider a mode-I crack propagating dynamically in a thin plate composed of a homogeneous isotropic, linear elastic solid. The crack-tip velocity and the dynamic stress intensity factor are both allowed to be arbitrary functions of time. If a *generalized plane stress* assumption is made, then the thickness averages of the stresses at the vicinity of the propagating crack are asymptotically proportional to $r^{-1/2}$, where r is the distance from the propagating crack tip. In particular, the thickness average of the first stress invarient $\hat{\sigma}_{11} + \hat{\sigma}_{22}$, which is of relevance in both CGS and caustics, is asymptotically given by:[15]

$$\hat{\sigma}_{11} + \hat{\sigma}_{22} = F(v) \frac{K_I^d(t)}{\sqrt{2\pi r_t}} \cos(\theta_t/2) + O(1) \quad \text{as} \quad r_t \to 0 \tag{6}$$

where

$$F(v) = \frac{2(1 + \alpha_s^2)(\alpha_t^2 - \alpha_s^2)}{[4\alpha_t\alpha_s - (1 + \alpha_s^2)^2]}$$

$$\alpha_{t,s} = \left(1 - \frac{v(t)^2}{c_{t,s}^2}\right)^{1/2}$$

$v(t)$ is the instantaneous crack speed; $c_{l,s}$ are the longitudinal and shear wave speeds, respectively; $K_I^d(t)$ is the instaneous value of the dynamic stress intensity factor;

$$r_l = (x_l^2 + (\alpha_l x_2)^2)^{1/2}; \qquad \theta_l = \tan^{-1}((\alpha_l x_2)/x_1)$$

and the distorted polar coordinate system (r_l, θ_l) translates with the moving crack tip. Stationary cracks in linear elastic solids are a special case for $v = 0$.

For laboratory specimens of finite dimensions, the above field can be valid only within a region near the crack tip of small extent compared with any relevant characteristic dimension of the body. On the other hand, the assumption of a two-dimensional field cannot be valid right up to the crack tip. As shown in the previous section, within some region near the tip (closer than half the specimen thickness) the two-dimensional field must give way to a region of severe three-dimensionality where the plane stress assumption breaks down. Although the above restrictions are *competing,* there may be cases where there is some finite annular region surrounding the crack tip such that the stress field is square-root singular and $(\hat{\sigma}_{11} + \hat{\sigma}_{22})$ is described by eqn (6). In such cases we say that we have a situation of K_I^d-*dominance* and we assume that the stress-intensity factor characterizes the fracture process. The classical analysis of caustics,[13] for both statics and dynamics, assumes that K_I^d-dominance always exists and attempts to relate the dimensions of the caustic curve to the instantaneous value of K_I^d.

From a mathematical standpoint, eqn (6) is only the leading term of a *transient asymptotic* expansion for the stresses, which will be presented in the following section. As will be seen in that section, only the leading $1/\sqrt{r_l}$ term of the transient expansion has the same form as the corresponding term of an expansion obtained if *steady-state* conditions are assumed. Indeed, the $O(1/\sqrt{r_l})$ term of the transient problem is obtained if the constant values for K_I^d and v of the steady-state case are replaced by their time-varying counterparts. However, this is not true for terms of higher order. For the transient crack-growth problem, such terms will in general contain time derivatives of $v(t)$ and $K_I^d(t)$. As a result, their importance relative to the leading term will depend on the nature of the time history of crack-tip speed and stress intensity factor as well as on the distances from the crack tip where measurements are performed. In addition, the θ_l variations of the transient higher-order terms are found to be different from their steady-state counterparts of the same order in r_l.

The situation in which the near-tip stresses are square-root singular

and, thus, eqn (6) provides an adequate representation of the first stress invarient at some annular region surrounding the crack tip is called one of *K_I^d-dominance.*

For the sake of analyzing CGS fringe patterns and in view of eqns (6), let us now define the quantities $Y_1^d(r_l, \theta_l, t)$ and $(Y_2^d(r_l, \theta_l, t)$, related to the x_1 and x_2 partial derivatives of $\hat{\sigma}_{11} + \hat{\sigma}_{22}$, as follows:

$$Y_\alpha^d(r_l, \theta_l, t) = \frac{\partial(\hat{\sigma}_{11} + \hat{\sigma}_{22})}{\partial x_\alpha} \cdot \frac{2\sqrt{2\pi}\, r_l^{3/2}}{F(v)\left[\delta_{1\alpha} \cos\frac{3\theta_l}{2} + \delta_{2\alpha} \sin\frac{3\theta_l}{2}\right]} \tag{7}$$

where $F(v)$, r_l, θ_l are as defined in eqn (6); $\delta_{\alpha\beta}$ is the Kronecker delta and α, β have the range $\{1, 2\}$. $Y_\alpha^d(r_l, \theta_l)$ are constructed by normalizing the actual x_1- and x_2-gradients of $\hat{\sigma}_{11} + \hat{\sigma}_{22}$, as measured by CGS, by the same gradients corresponding to the asymptotic field of eqn (6) divided by the stress intensity factor. In time instants such that K_I^d-dominance prevails (i.e. times such that there exist regions near the crack tip where eqn (6) describes the stress field), $Y_\alpha^d(r_l, \theta_l)$ are both equal to $K_I^d(t)$, for any choice of r_l and θ_l within the region of K_I^d-dominance. At time instants during crack growth such that K_I-dominance fails (the K_I^d-dominant region vanishes), $Y_\alpha^d(r_l, \theta_l, t)$ are not in general constant but rather are expected to be functions of position.

For situations of K_I^d-dominance, eqn (7) can be used to estimate the stress-intensity factor from CGS fringes by observing that use of eqns (5) and (6) results in the following relations for $K_I^d(t)$:

$$K_I^d(t) = Y_\alpha^d(r_l, \theta_l, t)$$

where

$$Y_\alpha^d(r_l, \theta_l, t) = \frac{k_\alpha p}{\Delta} \cdot \frac{2\sqrt{2\pi}\, r_l^{3/2}}{chF(v)\left[\delta_{1\alpha} \cos\frac{3\theta_l}{2} + \delta_{2\alpha} \sin\frac{3\theta_l}{2}\right]} \tag{8}$$

$$k_\alpha = \begin{Bmatrix} m \text{ for } \alpha = 1,\ m = 0, \pm 1, \pm 2, \ldots \\ n \text{ for } \alpha = 2,\ n = 0, \pm 1, \pm 2, \ldots \end{Bmatrix}$$

$$c = \begin{Bmatrix} c_\sigma, \text{ for } \textit{transmission} \\ -\nu/E \text{ for } \textit{reflection} \end{Bmatrix}$$

The right-hand side of eqn (8) can be experimentally measured from a CGS interferogram. Δ, p, c and h are constants related to the experimental set-up material and specimen. Also, if $v(t)$ is known, r_l, θ_l

can be computed from the position (r, θ) of *any point within the* K_I^d-dominant region while m or n are fringe orders.

EXPERIMENTAL INVESTIGATION OF K_I^d-DOMINANCE

The question of K_I^d-dominance has been investigated in detail by Tippur *et al.*,[2] Krishnaswamy *et al.*,[8] and by Freund and Rosakis[9] for both the quasistatic and dynamic cases by using the method of CGS. Here we present a summary of their results. Our goal is not only to observe situations of lack of K_I^d-dominance but also to examine the nature of the near-tip field when this assumption fails. Our specific aim is to verify the hypothesis of Freund and Rosakis[9] regarding the validity of a higher-order transient elastodynamic expansion for the near-tip deformation field. We begin our experimental investigation of this phenomenon by considering a set of experiments performed on precracked PMMA and AISI-4340 steel specimens in both transmission and reflection modes.

The specimen geometry was of the three-point bend type. The nominal specimen dimensions were length $2l = 30{\cdot}4$ cm, width $w = 12{\cdot}7$ cm and thickness $h = 1$ cm. A band saw, approximately 0·75 mm thick, was used to cut an initial notch of length $a = 25$ mm in these specimens. In the transmission mode, no further specimen preparation was needed. In the reflection mode, an aluminimum coating was applied to the PMMA specimen surface through a vacuum deposition technique in order to make it reflective. The 4340 carbon steel specimens were lapped so that their surfaces became optically flat. Then they were polished by a diamond paste to a mirror finish. An aluminum coating was also applied to increase the reflectivity.[8]

The specimens were loaded in a three-point bending configuration. The loading device used to dynamically load the specimens was the Dynatup 8100A drop-weight tower. The experimental configuration is such that the crack is under mode-I loading conditions.

A rotating-mirror type, high-speed camera set-up was used to obtain a sequence of dynamics CGS interferograms. A Spectra Physics (model 166) argon-ion pulse laser (output power 2W at $\lambda = 514$ nm in continuous wave mode) was used as the light source. The later beam was expanded and collimated to obtain a beam 50 mm in diameter which was centered on the initial notich tip of the specimen. The transmitted or reflected object wave-front was then processed through a pair of line gratings of density 40 lines/mm with a separation distance $\Delta = 30$ mm.

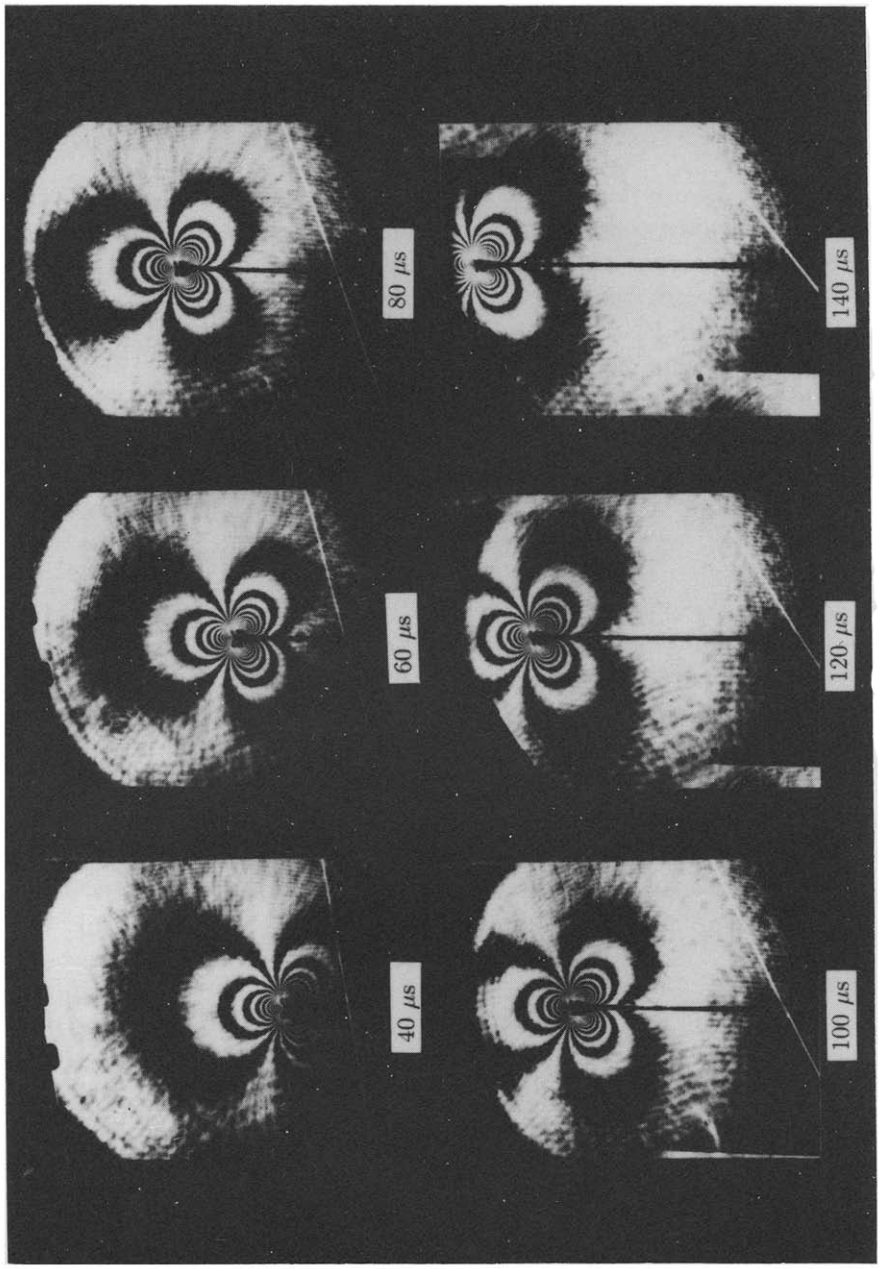

Fig. 3. Sequence of transmission CGS $|x_1$-gradient fringe patterns for a dynamically propagating crack in a PMMA specimen.

The gratings were oriented with their principal direction parallel to the crack line in order to obtain the x_1-gradient information of the crack-tip fields. The resulting diffraction wave fronts were then collected, filtered and imaged onto a rotating-mirror high-speed camera through a series of lenses. The pulsing circuit of the laser was set to give 50 ns exposure every 5 to 10 μs for a total of 1 ms from the time of an input trigger, which was synchronized to the moment of impact of the drop-weight with the specimen.

Figure 3 shows a representative sequence of CGS (transmission mode) interferograms for the case of a dynamically propagating crack in a PMMA specimen. Figure 4 shows a CGS pattern corresponding to a time 20 μs after initiation.

It was found that the crack propagated with an essentially constant velocity of about 0·3 the shear wave speed of the material. These fringe patterns correspond to the case when the diffraction gratings were oriented with their principal directions parallel to the x_1-axis. Thus, the

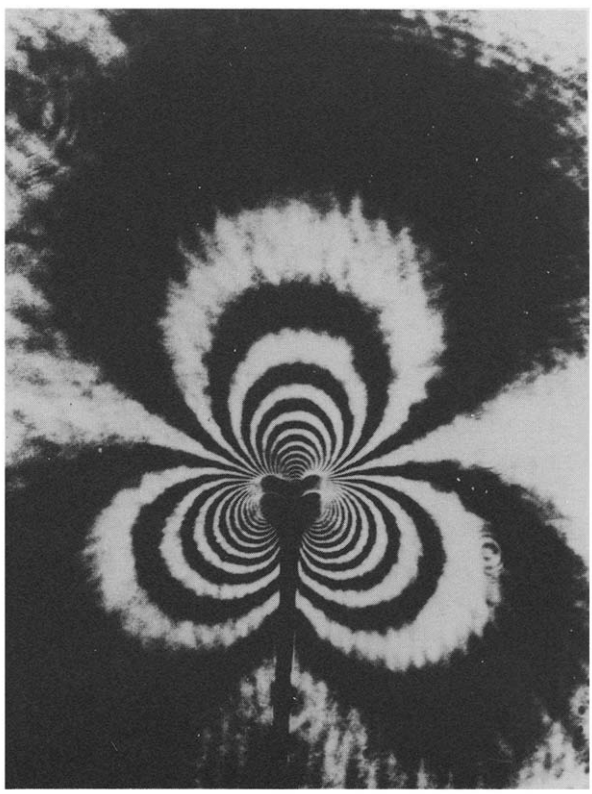

Fig. 4. Transmission CGS, x_1-gradient pattern (enlarged). The crack propagation direction is x_1. time is 20 μs after initiation.

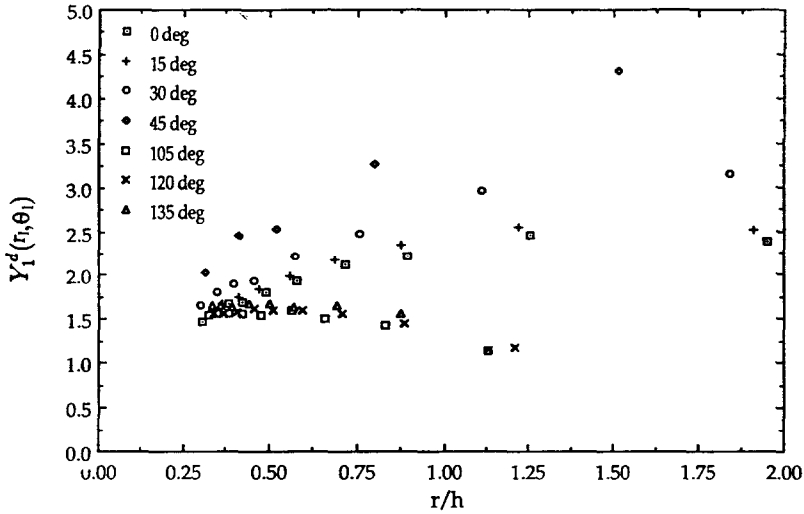

Fig. 5. Radial variation of $Y_I^d(r, \theta)$ along various values of θ for a dynamically propagating crack in a PMMA, corresponding to $20\,\mu s$ from crack initiation, when crack length to plate width ratio is instantaneously equal to $a/w = 0{\cdot}2$.

fringes surrounding the crack-tip at each instant of time represent the x_1-gradient of ΔS. In regions where plane stress conditions prevail, fringes are proportional to the x_1-gradient of $\hat{\sigma}_{11} + \hat{\sigma}_{22}$.

The fringe patterns were digitized for analysis to get fringe order (m) and location (r_l, θ_l) with respect to the crack -tip at each instant in time. The quantity $Y_I^d(r_l, \theta_l, t)$, defined in eqn (7), can now be plotted from the experimental data obtained from each CGS interferogram. If the field if K_I^d-dominant $Y_I^d(r_l, \theta_l, t)$ should be a constant $\forall(r, \theta)$ and equal to K_I^d.

Figure 5 shows a typical plot of Y_I^d against normalized radial distance (r/h) for one particular specimen for a time instant a few microseconds after crack initiation and for different radial lines $\theta_1 = 0°$, 15°, 30°, 45°, 105°, 120° and 135° around the propagating crack tip.

The crack tip velocity at that time is approximately $300\,m/s$. As is apparent from Fig. 5, there appears to be *no* region around the crack tip over which the function Y_I^d is consistant. Indeed, the spread in Y_I^d values from different locations is as much as 400%. Obviously, extraction of the dynamic stress-intensity factor value cannot be based here on a simplistic assumption of near-tip K_I^d-dominance; see eqn (8) for $K_I^d(t)$. One other interesting point must be made. The instantaneous crack length a to plate width w ratio at the time shown in Fig. 5 was $a/w = 0{\cdot}2$. The immediate question that arises is: Would there be a region of *static* K_I-dominance around a stationary crack of the same

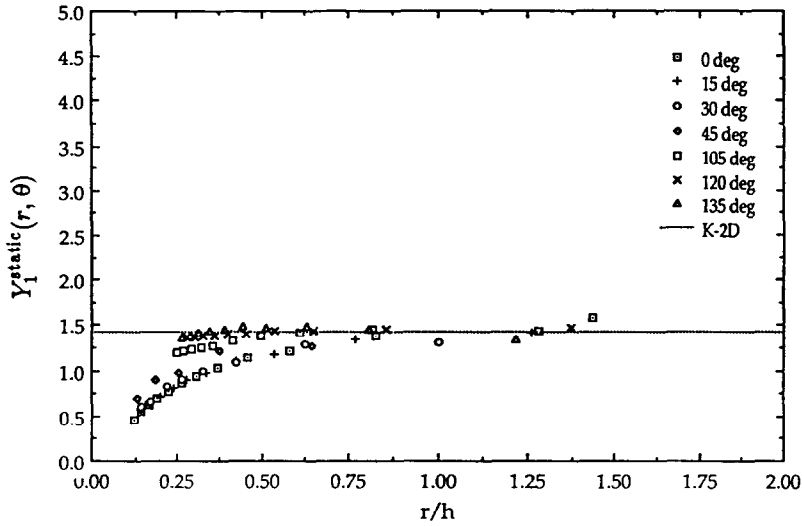

Fig. 6. Radial variation of $Y_I^{static}(r, \theta)$ along various values of θ for a statically loaded crack in a PMMA specimen with crack length to plate width ratio of $a/w = 0{\cdot}2$.

length in a *statically* loaded specimen of the *same* geometry? The answer is provided in Fig. 6, which shows a plot of the static counterparts of the quantities plotted in Fig. 5 for the case of a specimen with $a/w = 0{\cdot}2$ in an identical specimen to the one tested dynamically.

In the region $(r/h) < 0{\cdot}5$, Y_I^{static} does not seem to be constant and, thus, the field in this region does not appear to be K_I-dominant. This is consistent with other experimental investigations using caustics, wherein such deviation has been attributed to near-tip three-dimensionality.[11] Outside this three-dimensional region, however, there appears to be a sizable region of constant Y_I^{static} in the range $0{\cdot}5 \leq (r/h) \leq 1{\cdot}25$. Further, the constant value of Y_I^{static} in this range is in good agreement with the static stress-intensity factor K_I^{2D} as obtained from boundary load measurements. This is a clear indication that even though a stationary crack might exhibit a sizable region of K_I-dominance under static loading conditions, there might be no corresponding region of K_I^d-dominance when a crack of the same *instantaneous* length is propagating dynamically in an identical specimen subjected to dynamic loading.

It should be noted at this point that the reflection experiments performed on PMMA and 4340 steel, reported by Krishnaswamy *et al.*,[8] corroborate the above conclusions. The results are entirely analogous.

The observed lack of dynamic K_I^d-dominance outside the near-tip

three-dimensional region using CGS is consistent with the observation of lack of K_I^d-dominance observed by Krishnaswamy and Rosakis,[16] by means of a bifocal caustics arrangement.

In the next section we provide an explanation of $Y_1^d(r_l, \theta_l)$ values presented in Fig. 5. Our goal is to demonstrate that the observed spread in Y_1^d values is governed by the *specific structure of the transient stress field* near the crack tip and is not due to random experimental error. Consequently, we investigate the interpretation of dynamic CGS fringes on the basis of a *transient* higher-order expansion.

INTERPRETATION OF CGS ON THE BASIS OF A HIGHER-ORDER TRANSIENT ELASTODYNAMIC ANALYSIS

While dynamic caustic patterns have traditionally been analyzed under the often unverified assumption of K_I^d-dominance, the use of higher-order terms has been recent practice in the method of dynamic photoelasticity (Dally *et al.*[17]). However, all available high-order elastodynamic solutions thus far have been for the case of steadily propagating cracks and the applicability of such solutions to *highly transient* problems may be questioned. Indeed, the main criticism of this approach has been that such a procedure may result in inappropraite time-averaging of field quantities. Nonetheless, use of a higher-order steady-state expansion in the analysis of optical data is bound to be an improvement over the assumption of strict K_I^d-dominance.

In the following, we will relax the assumptions of near-tip K_I^d-dominance and steady-state crack propagation. We will show that if these assumptions fail, the experimentally obtained transmission and reflection mode CGS interferograms can be successfully interpreted on the basis of a transient, higher-order stress field for a propagating crack that has become available recently (Freund and Rosakis;[9] Rosakis *et al.*[10]). This procedure allows for the accurate measurment of $K_I^d(t)$ even in the presence of highly transient crack growth events.

TRANSIENT HIGHER-ORDER FIELDS

Freund and Rosakis and Rosakis *et al.* have extended the earlier interior asymptotic solution of Freund and Clifton to provide a higher-order description of the transient stress-state at the vicinity of a dynamically propagating crack. The most general form of this expansion corresponding to non-uniform crack velocities and stress intensity factor histories is briefly discussed below.

Consider a planar, mode-I crack that grows dynamically through a two-dimensional homogeneous, isotropic, linearly elastic solid, which a non-uniform speed $v(t)$, along the positive x_1-direction; $(0; x_1, x_2)$ is a proper orthogonal coordinate frame which translates with the non-uniformly moving crack tip. In terms of the displacement potential functions $\Phi(x_1, x_2, t)$ and $\Psi(x_1, x_2, t)$ the equations of motion in the absence of body forces can be expressed as

$$\left(1-\frac{v^2(t)}{c_l^2}\right)\frac{\partial^2\Phi}{\partial x_1^2}+\frac{\partial^2\Phi}{\partial x_2^2}+\frac{\dot{v}(t)}{c_l^2}\frac{\partial\Phi}{\partial x_1}+\frac{2v(t)}{c_l^2}\frac{\partial^2\Phi}{\partial x_l\,\partial t}-\frac{1}{c_l^2}\frac{\partial^2\varphi}{\partial t^2}=0 \tag{9}$$

$$\left(1-\frac{v^2(t)}{c_s^2}\right)\frac{\partial^2\Psi}{\partial x_1^2}+\frac{\partial^2\Psi}{\partial x_2^2}+\frac{\dot{v}(t)}{c_s^2}\frac{\partial\Psi}{\partial x_1}+\frac{2v(t)}{c_l^2}\frac{\partial^2\Psi}{\partial x_1\,\partial t}-\frac{1}{c_s^2}\frac{\partial^2\Psi}{\partial t^2}=0$$

where c_l and c_s are the longitidinal and shear wave speeds, respectively.

For the special case of constant velocity crack growth $\dot{v}=0$, the third term of eqns (9) vanishes while the last two terms are in general retained. In such a case, one speaks of constant velocity transient growth where an observer moving with the crack tip may still observe time changes in field quantities even if $\dot{v}(t)=0$. If in addition to $\dot{v}(t)=0$ also $\partial/\partial t\Phi(x_1, x_2, t)=0$ and $\partial/\partial t\Psi(x_1, x_2, t)=0$, then we speak of steady-state conditions and the above equations reduce Laplaces equations for Φ and Ψ with respect to the scaled coordinate system $(x_1, \alpha_{l,s}, x_2)$ (first two terms of eqns (9)). The higher-order expansion for Φ and Ψ that appears in Dally *et al.*[17] corresponds to the solution of these scaled Laplace equations.

Here we discuss a higher-order expansion where none of the simplications are used. Indeed, for the general transient crack-growth case, Freund and Rosakis[9] and Rosakis *et al.*[10] have expanded Φ and Ψ in powers of $r=\sqrt{(x_1^2+x_2^2)}$ substituted in a complete version of relation (9) and obtained expressions for the asymptotic stress field. In what follows, expressions for σ_{11}, σ_{22} and σ_{12} are given up to the third term in r as follows:

$$\sigma_{11}=\frac{K_1^d(t)}{\sqrt{2\pi}}\frac{1}{D}\left\{(1+2\alpha_l^2-\alpha_s^2)(1+\alpha_s^2)r_l^{-1/2}\cos\frac{\theta_l}{2}-4\alpha_l\alpha_s r_s^{-1/2}\cos\frac{\theta_s}{2}\right\}$$
$$+2\mu\left\{\frac{2(\alpha_l^2-\alpha_s^2)(1+\alpha_s^2)}{D}-1\right\}A_1(t)$$
$$+\mu\left\{\left[\frac{15(1+2\alpha_l^2-\alpha_s^2)(1+\alpha_s^2)}{4D}A_2(t)\right.\right.$$
$$+\left(\frac{\alpha_l^2(\alpha_l^2-\alpha_s^2)}{1-\alpha_l}+\frac{3(1-\alpha_s^2)-2\alpha_l^2}{8}\right)$$

$$\times D_I^1\{A_0(t)\} + \frac{1}{2}\left(\frac{\alpha_I^2(\alpha_I^2-\alpha_s^2)}{1-\alpha_I^2} - \frac{11(1-\alpha_s^2)+38\alpha_I^2}{16}\right)B_I(t)\Bigg]\cos\frac{\theta_I}{2}$$

$$+\left[\frac{1+2\alpha_I^2-\alpha_s^2}{8}D_I^1\{A_0(t)\} - \frac{1}{2}\left(\frac{\alpha_I^2(\alpha_I^2-\alpha_s^2)}{1-\alpha_I^2} + \frac{3(1-\alpha_s^2)-2\alpha_I^2}{8}\right)B_I(t)\right]$$

$$\times\cos\frac{3\theta_I}{2} + \frac{1+2\alpha_I^2-\alpha_s^2}{8}B_I(t)\cos\frac{7\theta_I}{2}\Bigg\}r_I^{1/2}$$

$$+2\mu\alpha_s\Bigg\{\Bigg[-\frac{15\alpha_I}{2D}A_2(t) - \frac{5-3\alpha_s^2}{8(1+\alpha_s^2)}D_s^1\{A_0(t)\} + \tfrac{13}{32}B_s(t)\Bigg]\cos\frac{\theta_s}{2}$$

$$+\tfrac{1}{8}(D_s^1\{A_0(t)\} + \tfrac{1}{2}B_s(t))\cos\frac{3\theta_s}{2} + \tfrac{1}{32}B_s(t)\cos\frac{7\theta_s}{2}\Bigg\}r_s^{1/2} + O(r_{I,s}) \qquad (10)$$

$$\sigma_{22} = \frac{K_I^d(t)}{\sqrt{2\pi}}\frac{1}{D}\left\{-(1+\alpha_s^2)^2 r_I^{-1/2}\cos\frac{\theta_I}{2} + 4\alpha_I\alpha_s r_s^{-1/2}\cos\frac{\theta_s}{2}\right\}$$

$$-\mu\Bigg\{\Bigg[\frac{15(1+\alpha_s^2)^2}{4D}A_2(t) - \left(\frac{\alpha_I^2-\alpha_s^2}{1-\alpha_I^2} - \frac{3-5\alpha_s^2}{8}\right)D_I^1\{A_0(t)\}$$

$$-\frac{1}{2}\left(\frac{\alpha_I^2-\alpha_s^2}{1-\alpha_I^2} + \frac{11+27\alpha_s^2}{16}\right)B_I(t)\Bigg]\cos\frac{\theta_I}{2}$$

$$+\left[\frac{1+\alpha_s^2}{8}D_I^1\{A_0(t)\} + \frac{1}{2}\left(\frac{\alpha_I^2-\alpha_s^2}{1-\alpha_I^2} - \frac{3-5\alpha_s}{8}\right)B_I(t)\right]\cos\frac{3\theta_I}{2}$$

$$+\frac{1+\alpha^{2s}}{32}B_I(t)\cos\frac{7\theta_I}{2}\Bigg\}r_I^{1/2}$$

$$-2\mu\alpha_s\Bigg\{\Bigg[-\frac{15\alpha_I}{2D}A_2(t) - \frac{5-3\alpha_s^2}{8(1+\alpha_s^2)}D_s^1\{A_0(t)\} + \tfrac{13}{32}B_s(t)\Bigg]\cos\frac{\theta_s}{2}$$

$$+\tfrac{1}{8}(D_s^1\{A_0(t)\} + \tfrac{1}{2}B_s(t))\cos\frac{3\theta_s}{2} + \tfrac{1}{32}B_s(t)\cos\frac{7\theta_s}{2}\Bigg\}r_s^{1/2} + O(r_{I,s}) \qquad (11)$$

$$\sigma_{12} = \frac{K_I^d(t)}{\sqrt{2\pi}}\frac{2\alpha_I^2(1+\alpha_s^2)}{D}\left\{r_I^{-1/2}\sin\frac{\theta_I}{2} - r_s^{-1/2}\sin\frac{\theta_s}{2}\right\}$$

$$-2\mu\alpha_I\Bigg\{\Bigg[\frac{15(1+\alpha_s^2)}{4D}A_2(t) - \tfrac{1}{8}D_I^1\{A_0(t) - \tfrac{3}{32}B_I(t)\Bigg]\sin\frac{\theta_I}{2}$$

$$-\tfrac{1}{8}(D_I^1\{A_0\} + \tfrac{1}{2}B_I(t))\sin\frac{3\theta_I}{2} - \tfrac{1}{32}B_I(t)\sin\frac{7\theta_I}{2}\Bigg\}r_I^{1/2}$$

$$-\mu\Bigg\{\Bigg[-\frac{15\alpha_I^2(1+\alpha_s^2)}{2D}A_2(t) - \frac{1+\alpha_s^2}{8}D_s^1\{A_0\} + \frac{5-11\alpha_s^2}{32}B_s(t)\Bigg]\sin\frac{\theta_s}{2}$$

$$-\left[\frac{1+\alpha_s^2}{8}D_s^1\{A_0(t)\} - \frac{3-5\alpha_s^2}{16}B_s(t)\right]\sin\frac{3\theta_s}{2} - \frac{1+\alpha_s^2}{32}B_s(t)\sin\frac{7\theta_s}{2}\Bigg\}r_s^{1/2}$$

$$+O(r_{I,s}) \qquad (12)$$

where

$$A_0(t) = \frac{4}{3\mu\sqrt{2\pi}} \frac{1+\alpha_s^2}{D(v)} K_I^d(t)$$

$$D_l^1\{A_0(t)\} = -\frac{3v^{1/2}(t)}{\alpha_l^2 c_l^2} \frac{d}{dt}\{v^{1/2}(t)A_0(t)\}$$

$$= -\frac{4v^{1/2}(t)}{\mu\sqrt{2\pi}\,\alpha_l^2 x_l^2} \frac{d}{dt}\left\{v^{1/2}(t)\frac{1+\alpha_s^2}{D(v)}K_I^d(t)\right\}$$

$$B_l(t) = \frac{3v^2(t)}{2\alpha_l^4 c_l^4} A_0(t) \frac{dv(t)}{dt}$$

$$= \frac{2v^2(t)}{\mu\sqrt{2\pi}\,\alpha_l^4 c_l^4} \frac{1+\alpha_s^2}{D(v)} K_I^d(t) \frac{dv(t)}{dt} \tag{13}$$

and

$$B_0(t) = -\frac{4}{3\mu\sqrt{2\pi}} \frac{2\alpha_l}{D(v)} K_I^d(t)$$

$$D_s^1\{B_0(t)\} = -\frac{3v^{1/2}(t)}{\alpha_s^2 c_s^2} \frac{d}{dt}\{v^{1/2}(t)B_0(t)\}$$

$$= \frac{4v^{1/2}(t)}{\mu\sqrt{2\pi}\,\alpha_s^2 c_s^2} \frac{d}{dt}\left\{v^{1/2}(t)\frac{2\alpha_l}{D(v)}K_I^d(t)\right\}$$

$$B_s(t) = \frac{3v^2(t)}{2\alpha_s^4 c_s^4} B_0(t)\, dv(t)\, dt$$

$$= -\frac{2v^2(t)}{\mu\sqrt{2\pi}\,\alpha_s^4 c_s^4} \frac{2\alpha_l}{D(v)} K_I^d \frac{dv(t)}{dt}$$

and

$$D(v) = 4\alpha_l\alpha_s - (1+\alpha_s^2)^2$$

and $A_1(t)$, $A_2(t)$ are functions of time undetermined by the asymptotic analysis.

In the above expressions, $A_0(t)$ is determined by the dynamic stress-intensity factor history, $K_I^d(t)$ and the propagating speed of the crack tip, $v(t)$; $D_l^1(A_0(t))$ and $D_s^1(A_0(t))$ depend not only on $K_I^d(t)$ and $v(t)$ but also on the time derivatives of these quantities. Besides $K_I^d(t)$ and $v(t)$, $B_l(t)$ and $B_s(t)$ also depend on the acceleration of the crack.

If the crack-tip speed $v(t)$ is a constant, i.e. $\dot{v}(t) = 0$ and, therefore, $B_l(t) = B_s(t) = 0$, we can obtain the asymptotic stress field corresponding to transient crack growth under constant velocity and varying stress intensity factor (Freund and Rosakis[9]). A classical example of such a

transient crack problem is the one analyzed by Broberg (see Freund[15]; Freund and Rosakis[9]). Furthermore, if the time derivative of the dynamic stress intensity factor, $K_I^d(t)$, it also zero, $D_1^1(B_0(t))$ will be zero; then we obtain the familiar results of the asymptotic stress field for the steady state up to three terms.

A useful special case of the above expansion is the one corresponding to transient but constant velocity crack growth. For the purpose of analyzing the constant velocity CGS experiments discussed above, we present here an higher-order expansion for $\hat{\sigma}_{11} + \hat{\sigma}_{22}$ corresponding to this case. This is given up to six terms as follows:

$$\begin{aligned}
\frac{\hat{\sigma}_{11}+\hat{\sigma}_{22}}{2\rho(c_l^2-c_s^2)} &= \frac{3v^2}{4c_l^2}A_0\cos(\theta_l/2)r_l^{-1/2} + \frac{2v^2}{c_l^2}A_1 \\
&+ \left[\left\{\frac{15v^2}{4c_l^2}A_2 + \left(1-\frac{v^2}{2c_l^2}\right)D^1(A_0)\right\}\cos(\theta_l/2) + \frac{v^2}{8c_l^2}D^1(A_0)\cos(3\theta_l/2)\right]r_l^{1/2} \\
&+ \left[\left\{\frac{6v^2}{c_l^2}A_3 + \left(1-\frac{v^2}{4c_l^2}\right)D^1(A_1)\right\}\cos(\theta_1)\right]r_l \\
&+ \left[\left\{\frac{35v^2}{4c_l^2}A_4 + \left(1-\frac{v^2}{2c_l^2}\right)D^1(A_2) + \frac{1}{9}\left(1+\frac{v^2}{4c_l^2}\right)D^2(A_0) + \left(1-\frac{v^2}{2c_l^2}\right)\ddot{A}_0\right\}\right. \\
&\times\cos(3\theta_l/2) + \left\{\frac{3v^2}{8c_l^2}D^1(A_2) + \frac{1}{6}\left(1-\frac{v^2}{4c_l^2}\right)D^2(A_0) + \frac{3v^2}{8c_l^2}\ddot{A}_0\right\} \\
&\times\cos(\theta_l/2) + \left\{\frac{v^2}{96c_l^2}D^2(A_0)\right\}\cos(5\theta_l/2)r \\
&+ \left[\left\{\frac{12v^2}{c_l^2}A_5 + \left(1-\frac{v^2}{2c_l^2}\right)D^1(A_3) + \frac{D^2(A_1)}{16} + \left(1-\frac{v^2}{2c_l^2}\right)\ddot{A}_1\right\}\cos(2\theta_l)\right. \\
&+ \left.\left\{\frac{v^2}{2c_l^2}D^1(A_3) + \frac{1}{8}\left(1-\frac{v^2}{4c_l^2}\right)D^2(A_1) + \frac{v^2}{2c_l^2}\ddot{A}_1\right\}r_l^2 + o(r_l^2)\right. \qquad (14)
\end{aligned}$$

and

$$D^1(A_k) = -\frac{(k+3)v}{c_l^2\alpha_l^2}\frac{\mathrm{d}}{\mathrm{d}t}(A_k), \qquad k = 0, 1, 2, \ldots,$$

$$D^2(A_k) = D^1(D^1(A_k)),$$

$$\ddot{A}_k = \frac{1}{c_l^2\alpha_l^2}\left(\frac{\mathrm{d}^2}{\mathrm{d}t^2}A_k\right)$$

and ρ is the mass density of the material. Although the above expression is for the special case of constant crack velocity, the

coefficients A_k in the above transient field are allowed to be time-varying as opposed to the steady-state approximation where the corresponding coefficients must be constant. Note also that only the terms associated with coefficients A_k are identical to the ones that would be obtained form a higher-order *steady-state* analysis with $A_0(t)$ being proportional to the dynamic stress intensity factor, and so on. Furthermore, it is seen that the higher-order transient expression contains *additional* terms whose coefficients depend on *time derivatives* of lower-order coefficients. As a result, the net spatial variation shown in the above expression is *different* from the steady-state higher-order expansion used by Dally *et al.*[17] An illustration of the interdependence of the coefficients of higher- and lower-order terms is provided if one observes that $D^1(A_0)$ is proportional to the first time derivative of the stress-intensity factor history, since

$$A_0(t) = \frac{4}{3}\frac{K_I^d(t)}{\pi\sqrt{2\pi}}\frac{(1+\alpha_s^2)}{[4\alpha_s\alpha_l - (1+\alpha_s^2)^2]} \tag{15}$$

Substituting the transient field given in eqn (14) into the x_1-gradient transmission-mode fringe eqn (5), and using eqn (7), we get an expression for $Y_I^d(r_l, \theta_l, t)$ of the form

$$\begin{aligned} Y_I^d(r_l, \theta_l, t) &= \left(\frac{mp}{\Delta}\frac{1}{F(v)}\frac{2\sqrt{2\pi}}{c_\sigma h}\frac{r_l^{3/2}}{\cos(3\theta_l/2)}\right) \\ &= K_I^d + \left\{\beta_2\frac{\cos(\theta_l/2)}{\cos(3\theta_l/2)} + \beta_3\frac{\cos(5\theta_l/2}{\cos(3\theta_l/2)}\right\}r_l \\ &\quad + \left\{\beta_4\frac{1}{\cos(3\theta_l/2)}\right\}r_l^{3/2} + \left\{\beta_4\frac{\cos(\theta_l/2)}{\cos(3\theta_l/2)} + \beta_6 + \beta_7\frac{\cos(7\theta_l/2)}{\cos(3\theta_l/2)}\right\}r_l^2 \\ &\quad + \left\{\beta_8\frac{\cos(\theta_l)}{\cos(3\theta_l/2)}\right\}r_l^{5/2} + O(r^3) \end{aligned} \tag{16}$$

where K_I^d, the dynamic stress-intensity factor, as well as $\beta_2 \cdots \beta_8$ are time-dependent coefficients to be determined. Under K_I^d-dominance, Y_I^d would have been a constant, for every (r_l, θ_l), and would be equal to the instantaneous stress-intensity factor K_I^d. If significant higher-order transient terms exist, then the variation of Y_I^d would be given by the right-hand side of eqn (16), which for simplicity will be denoted by $G_I^d(r_l, \theta_l; K_I^d, \beta_2 \cdots \beta_8)$.

A least-squares procedure analogous to the one described by Tippur *et al.* was used to fit the above function G_I^d to the experimental data Y_I^d obtained from the CGS interferograms. Since eqn (16) is obtained from

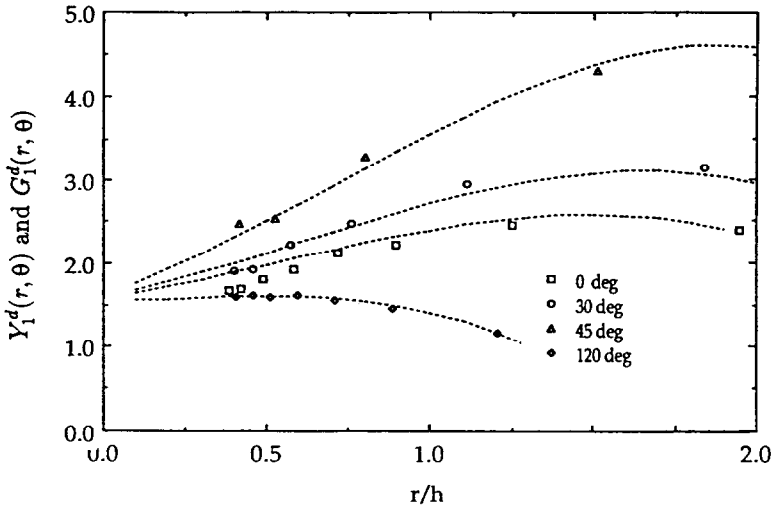

Fig. 7. Comparison of the radial variation of the experimental data $Y_1^d(r, \theta)$ and the analytical fit $G_1^d(r, \theta)$ for various values of θ for the same data presented in Fig. 5.

a two-dimensional analysis, data from the near-tip three-dimensional region were excluded. The three-dimensional region excluded was based on a cut-off value for the degree of plane strain (which, strictly, should be zero in regions of plane stress) as shown in Fig. 2.

Figure 7 shows the results for one particular time instant during crack propagation in a specimen 20 μs after crack initiation. The agreement between the fitted function G_1^d (based on the transient expansion (15) to $O(r^2)$) and the experimental data in Fig. 7 is seen to be remarkably good. It is seen that the transient analysis agrees very well with the experimental data in the range $(0{\cdot}5 < r/h < 2{\cdot}0, -\pi < \theta < \pi)$, whereas the K_1^d-dominance assumption is clearly inadequate. This was the case for most interferograms obtained at times close to crack initiation.

This strongly suggests that *the observed lack of K_1^d-dominance in the two-dimensional region outside the near-tip three-dimensional zone is due to the important contribution of higher-order terms to the total stress and deformation fields around the crack tip. The importance of these terms relative to the first term of the expansion is found to be intimately related to the transient nature of the crack-growth event.*

Equivalent conclusions can be obtained when CGS is applied to the investigation of crack growth in opaque materials (see Ref. 8).

To further illustrate the *transient* nature of the crack-tip fields, the time histories of the stress-intensity factor $K_1^d(t)$ and of the coefficients $\beta_k(t)$ inferred from the data during a representative dynamic fracture

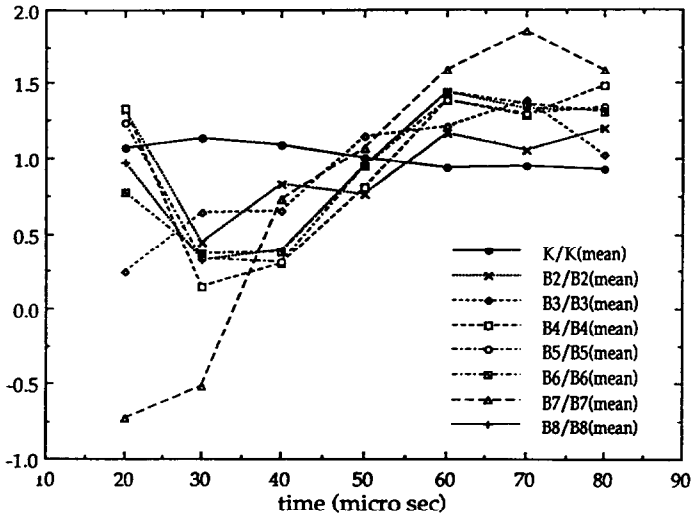

Fig. 8. Time histories of $K_I^d(t)$ and $\beta_k(t)$, each normalized by its mean value, for the duration of a particular crack-propagation event. (Crack growth in PMMA.)

experiment are shown in Fig. 8. Each of the quantities are normalized by means value for the entire test. Even though the crack speed was very uniform during the entire observations, Fig. 8 clearly shows the transient nature of the crack-growth process. For at least the first 50 μs after initiation of a crack growth from a stationary blunted notch, there is significant fluctuation in the values of $\beta_k(t)$, $k = 2, \ldots, 7$.

Figure 8 clearly shows the inadequacy of a *steady-state* higher-order expansion at times less than approximately 50 μs after initiation. As evident from the above results, the assumption of K_I^d-dominance may fail in the plane stress region surrounding the near-tip three-dimensional zone. This is expected to be true at times shortly after initiation or during the arrival of stress waves from the specimen boundaries when transient effects increase the importance of the higher-order terms relative to the singular term of the asymptotic expansion. This phenomenon is expected to influence the interpretability of other optical techniques applied to dynamic fracture, such as photoelasticity and caustics. For caustics, for example, it is expected that optical caustic patterns obtained from near-tip regions and analyzed by using the classical K_I^d-dominant analysis (see Rosakis and co-workers[14] and Beinert *et al.*[13]] would not necessarily yield the correct value of stress-intensity factor. (For an improved analysis of caustics using the transient higher-order expansion presented above, see Liu *et al.*[12])

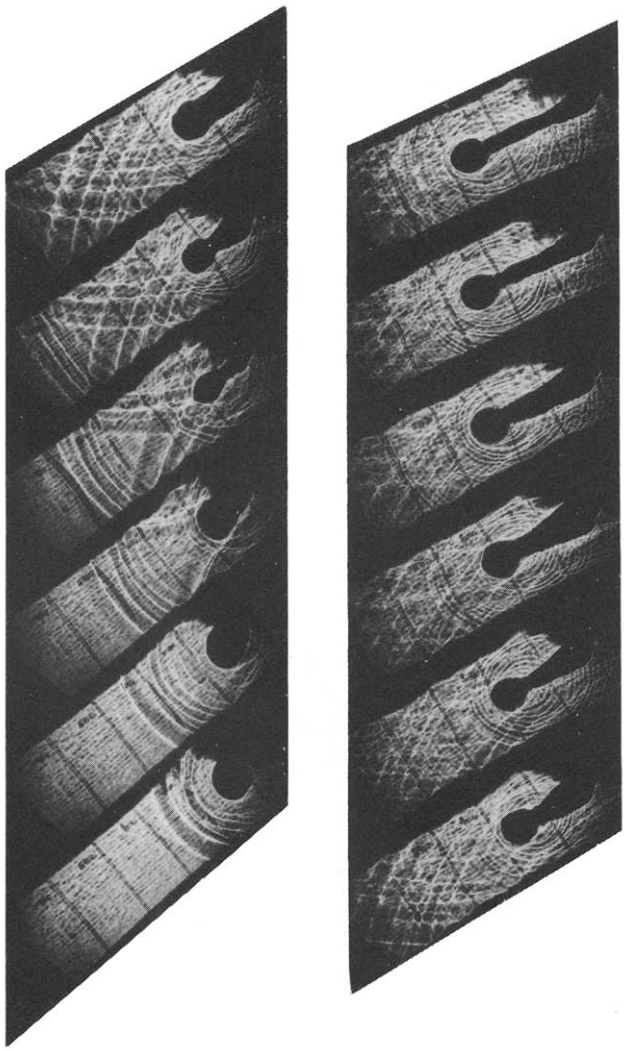

Fig. 9. Effect of wave reflection on caustic shape. A visual demonstration of the destruction of K_I^d-dominance by transients. Material, AISI-4340 steel; specimen, double cantilever beam.

A visual illustration of the effects of transients on the shape of the optical caustics is shown in Fig. 9. Here a crack is propagating dynamically in a wedge loaded, 'narrow', double cantilever beam specimen which acts as a wave guide. As the crack initiates, unloading waves, visible as bright lines, are generated (first two frames). The waves are reflected from the specimen sides and interact with the propagating crack tip, distorting the caustic shape (third to seventh

frames). After this time, multiple wave reflections help create a less transient environment in the specimen and the caustic curve attains a shape more closely resembling that predicted by K_I^d-dominant analysis. Although the above example is clearly *extreme* compared with crack growth in a large three-point bend specimen where wave reflections are not so important, it helps visualize the effect of transients in destroying K_I^d-dominance.

The experimental and theoretical results summarized above lead us to the following general conclusion regarding experimental dynamic crack-growth studies:

'Contrary to conventional wisdom, *strict* K_I^d-dominance in the vicinity of dynamically propagating crack tips appears to be the exception rather than the rule. It is thus critically important that interpretation of the experimental data under assumed K_I^d-dominance, steady-state or two-dimensional conditions be carefully justified prior to attributing physical credence to the observed phenomena.'

This observation may have important consequences in resolving a number of controversies that have arisen in experimental dynamic fracture studies of the recent past. In particular, this realization may be relevant in the resolution of the debate concerning the existence of a unique relation between dynamic fracture toughness and crack-tip velocity (uniqueness of the K_I^d versus v relation). For further discussion on this point see Refs 9 and 12.

APPLICATION OF CGS TO THE INVESTIGATION OF DYNAMIC FRACTURE IN BIMATERIAL INTERFACES

In this section we describe the initial steps of an investigation aimed towards the understanding of the mechanics of dynamic crack initiation and growth in bimaterial interfaces. Our goal is to perform direct optical near-tip dynamic measurements of deformation fields in real time and to study the effects of inertia and rate sensitivity on the initiation and propagation throughness of bimaterial systems. Here we report on our initial investigation regarding the interpretability of CGS fringes obtained at the vicinity of cracks in bimaterial interfaces. We concentrate on the influence of near-tip three-dimensionality on the interpretation of the optical patterns. Our aim is to identify regions near the tip where existing two-dimensional theories may facilitate the inference of relevant fracture parameters. We also present the results of some preliminary dynamic crack growth experiments in impact-loaded PMMA–Al specimens and PMMA–steel specimens.

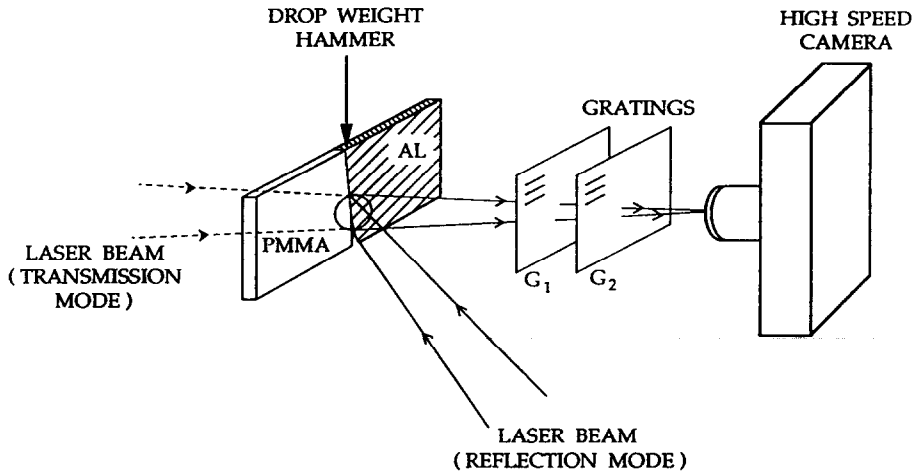

Fig. 10. Experimental arrangement for dynamic crack growth in bimaterial interfaces.

The specimen configuration is of the three-point bend type and is shown in Fig. 10. The bimaterial combinations tested were those of Al and PMMA and of steel and PMMA. Initial cracks existed on the bottom of the specimen along the bond line. In the dynamic experiments the specimens were impacted by means of a drop-weight tower.

DATA ANALYSIS

The data analysis in this case proceeds in a similar manner to the one described above for the homogeneous case. As noted there, it is very important to first identify the regions near the crack tip where a two-dimensional asymptotic field dominates. Once this is achieved, available analytical two-dimensional descriptions of the deformation field can be used to extract the relevant dynamic fracture quantities.

We start by considering the nature and extend of the near-tip three-dimensional zone for the case of a crack in the PMMA–Al interface, three-point bend bimaterial specimens. In what follows we present three-dimensional numerical results for the ratio $\sigma_{33}/\nu_\alpha(\sigma_{11}+\sigma_{22})$ $\alpha=(1,2)$, at the vicinity of the crack tip. In this expression, ν_1 and ν_2 correspond to the Poisson's ratio in the PMMA and Al parts of the specimens, respectively.

In Fig. 11 the ratio is plotted for the specimen mid-plane. The top side corresponds to PMMA and the crack line is visible in the left-hand side of the picture. Figure 12 gives a three-dimensional view of the PMMA side which is relevant for the analysis of the transmission CGS

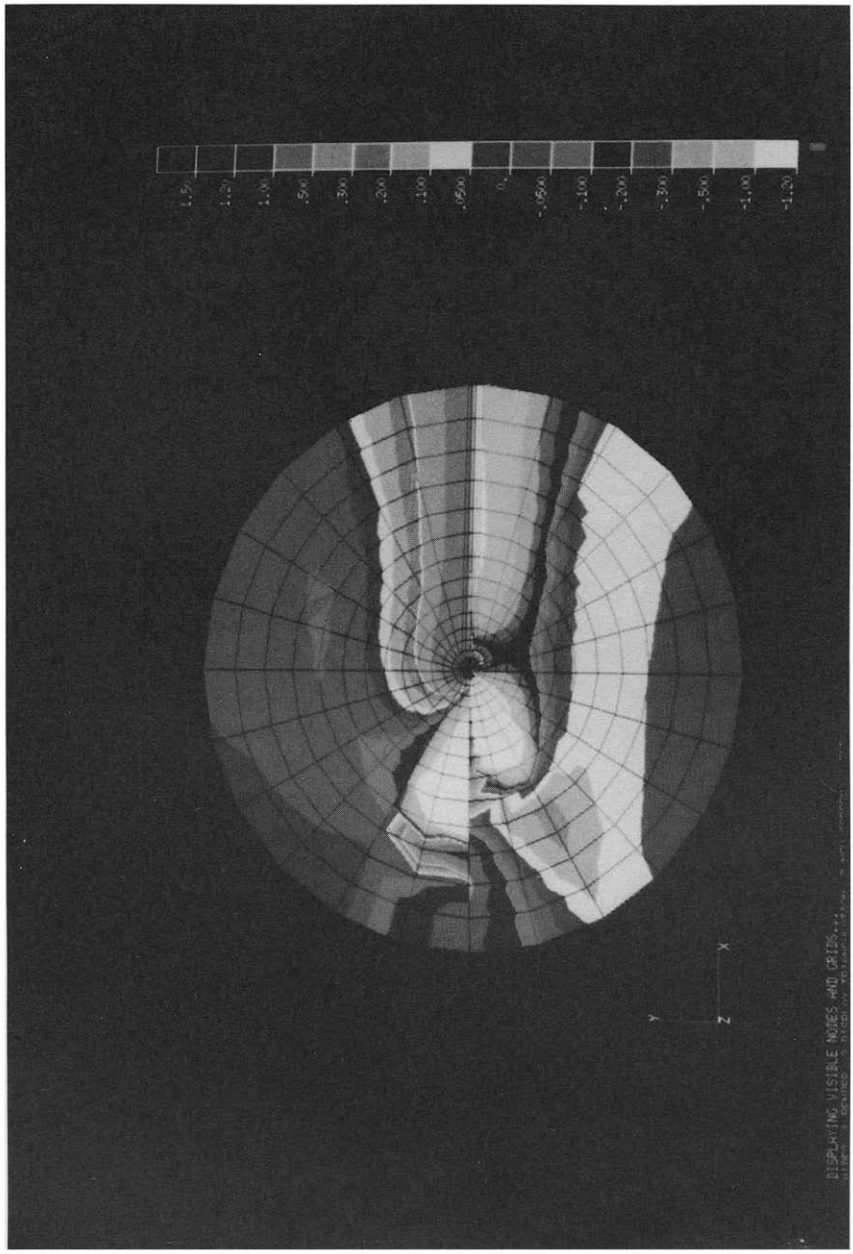

Fig. 11. View of the ratio $\sigma_{33}/\nu_\alpha(\sigma_{11}+\sigma_{22})$ in the mid-plane of a PMMA–Al three-point bend fracture specimen. Top, PMMA; Bottom, Al. The crack face is on the left-hand side. (From Lee and Rosakis[18].)

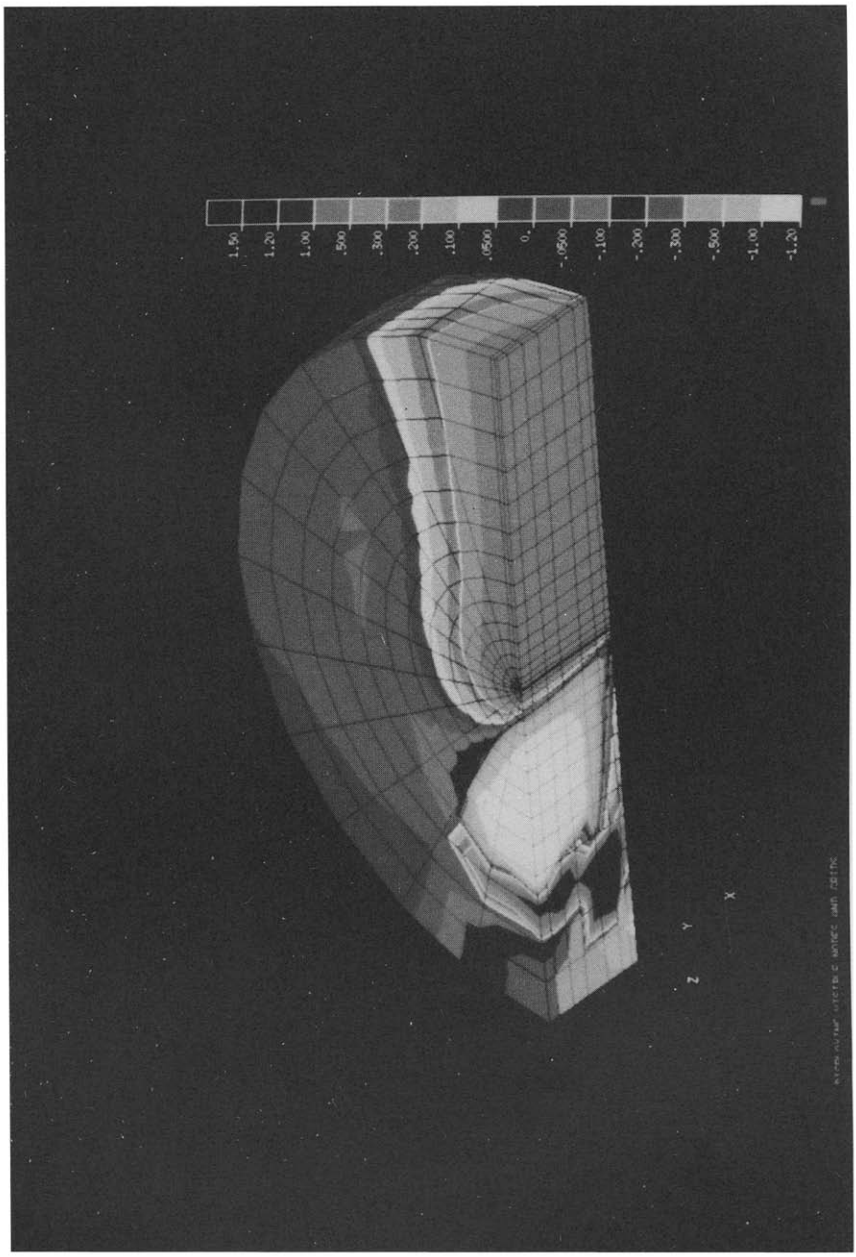

Fig. 12. Three-dimensional representation of the ratio $\sigma_{33}/\nu_1(\sigma_{11}+\sigma_{22})$ for a through crack in a PMMA–Al specimen. Only the PMMA side is shown. The crack face is on the left-hand side.

patterns. As is obvious from a comparison of Figures 2 and 12, the nature of the three-dimensional deformation of bimaterials is different from that of homogeneous systems. The top surface of the three dimensional mesh corresponds to the specimen mid-plane. As is obvious from Figs 11 and 11, the three-dimensional zone extends along the PMMA–Al bond line. Unlike the homogeneous case, there exists no plane stress region at any visible distance directly ahead to the crack tip. Here, plane stress conditions are achieved above a strip of height roughly equal to 0·4 h lying ahead of the tip in the PMMA side. In addition, there exists a narrow wedge of plane stress defined by $100° < \theta < 150°$, $r < 0{\cdot}1$ h. (For details see Lee and Rosakis[18].)

For points out the three-dimensional region, a plane stress approximation will be applicable ($\sigma_{33}/\nu_1(\sigma_{11}+\sigma_{22}) \to 0$). Indeed for such points the optical path difference for the PMMA side, ΔS_1 (eqn (2) which involves the ratio $\sigma_{33}/\nu_1(\sigma_{11}+\sigma_{22})$ will simplify to

$$\Delta S_1 = ch(\hat{\sigma}_{11} + \hat{\sigma}_{22})$$

For cracks propagating dynamically in bimaterial specimens, Yang *et al.*[19] observed that near the crack tip the stress field assumes the form

$$\hat{\sigma}_{\alpha\beta} = \mathrm{Re}\left\{\frac{K^{\mathrm{d}} r^{i\varepsilon}}{\sqrt{2\pi r}}\right\} \tilde{\sigma}^{(1)}_{\alpha\beta}(\theta, v) + \mathrm{Im}\left\{\frac{K^{\mathrm{d}} r^{i\varepsilon}}{\sqrt{2\pi r}}\right\} \tilde{\sigma}^{(2)}_{\alpha\beta}(\theta, v) \tag{17}$$

where r, θ, are polar coordinates of a coordinate system translating with the crack tip at velocity v and $K^{\mathrm{d}} = K_1^{\mathrm{d}} + iK_2^{\mathrm{d}}$ is the *complex dynamic* stress-intensity factor. The oscillatory index $\varepsilon = \hat{\varepsilon}(v)$ is now a function of crack-tip speed and the moduli of the materials of the bimaterial combination. Analytical expressions for $\tilde{\sigma}^{(1)}_{\alpha\beta}$ and $\tilde{\sigma}^{(2)}_{\alpha\beta}$ are given by Yang *et al.*[19]

By using eqn (17) and after some algebraic manipulation, $\hat{\sigma}_{11} + \hat{\sigma}_{22}$ can be written as

$$\hat{\sigma}_{11} + \hat{\sigma}_{22} = \frac{A}{\sqrt{2\pi r_l}} \cdot \left[(1 + \alpha_s^2 - 2\eta\alpha_s) \exp\left[\varepsilon(\pi - \theta_l)\right] \cos\left(\frac{\theta_l}{2} - \phi - \varepsilon \ln r_l\right)\right.$$
$$\left. + (1 + \alpha_s^2 + 2\eta\alpha_s) \exp\left[-\varepsilon(\pi + \theta_l)\right] \cos\left(\frac{\theta_l}{2} + \phi + \varepsilon \ln r_l\right)\right], \qquad r \to 0, \quad 0 \le \theta \le \pi \tag{18}$$

where

$$A = \frac{(\alpha_l^2 - \alpha_s^2)\,|K^{\mathrm{d}}|}{(4\alpha_l\alpha_s - (1 + \alpha_s^2)^2) \cosh \varepsilon\pi}$$

$$\alpha_{l,s} = \left(1 - \frac{v^2}{c_{l,s}}\right)^{1/2}, \qquad \theta_l = \tan^{-1}\left[(\alpha_l x_2)/x_1\right], \qquad r_l = (x_1^2 + \alpha_l^2 x_2^2)^{1/2}$$
$$K^2(t) = K_1^{\mathrm{d}}(t) + iK_2^{\mathrm{d}}(t), \qquad \phi(t) = \tan^{-1}\left(K_2^{\mathrm{d}}(t)/K_1^{\mathrm{d}}(t)\right)$$

$c_{l,s}$ are the longitudinal and transverse wave speeds, respectively; and $\varepsilon = \hat{\varepsilon}(v)$, $\eta = \hat{\eta}(v)$, are functions of the crack-tip speed and of the moduli of the materials involved in the bimaterial combination. These functions are given by Yang *et al.*[19] and are such that $\varepsilon \to \varepsilon_0$, $\eta \to 1$ and $v \to 0$. The bimaterial constant ε_0 is called the 'quisistatic' mismatch parameter and is given by

$$\varepsilon_0 = \frac{1}{2\pi} \ln \left[\frac{\dfrac{k_1}{\mu_1} + \dfrac{1}{\mu_2}}{\dfrac{k_2}{\mu_2} + \dfrac{1}{\mu_1}} \right]$$

where $k_\alpha = (3 - \nu)/(1 + \nu_\alpha)$ for plane stress and ν_α and μ_α are the Poisson's ratio and shear moduli for material 1 and material 2, respectively.

It should be emphasized here that as $v \to 0 (\eta \to 1, \alpha_l \to 1)$, $1 + \alpha_l^2 - 2\eta\alpha_l$ vanishes and eqn (18) becomes

$$\hat{\sigma}_{11} + \hat{\sigma}_{22} = \frac{2 \exp [\varepsilon_0(\theta - \pi)]}{\sqrt{2\pi r} \cosh (\pi\varepsilon)}$$

$$\times \left[K_1 \cos \left(\frac{\theta}{2} + \varepsilon \ln r \right) - K_2 \left(\frac{\theta}{2} + \varepsilon \ln r \right) \right], \qquad r \to 0,$$

where $K_1 = |K| \cos \phi$, $K_2 = |K| \sin \phi$. This is the expression appropriate for the analysis of CGS patterns in quasistatic bimaterial crack problems as described by Tippur and Rosakis.[20]

Also when the bimaterial system approaches the homogeneous limit $\varepsilon = 0$ and since growing cracks in a homogeneous material can only be of the mode-I type, ($\phi = 0$), then eqn (18) reduces to

$$\hat{\sigma}_{11} + \hat{\sigma}_{22} = \frac{2K_I^d(\alpha_l^2 - \alpha_s^2)(1 + \alpha_s^2)}{(4\alpha_l\alpha_s - (1 + \alpha_s^2)^2)} \frac{\cos (\theta_l/2)}{\sqrt{2\pi r_1}}, \qquad r \to 0$$

which is the expression appropriate for the analysis of CGS patterns for the case of elastodynamic crack growth in *homogeneous* materials (see Rosakis[5]).

The field quantity of interest in analyzing the CGS patterns in material 1 is $ch\,\partial(\hat{\sigma}_{11} + \hat{\sigma}_{22})/\partial x_1$. By differentiating eqn (18) with respect to x_1 we have

$$ch \frac{\partial(\hat{\sigma}_{11} + \hat{\sigma}_{22})}{\partial x_1} = \frac{chr_l^{-3/2} \exp (-\varepsilon(\pi - \theta_l))A}{2\sqrt{2\pi}}$$

$$\times \left[(1 + \alpha_s^2 - 2\eta\alpha_s) \exp [2\varepsilon(\pi - \theta_l)] \cos \left(\frac{3\theta_l}{2} - \phi - \varepsilon \ln r_l \right) \right.$$

$$- (1 + \alpha_s^2 + 2\eta\alpha_s) \cos\left(\frac{3\theta_l}{2} + \phi + \varepsilon \ln r_l\right)$$
$$+ 2\varepsilon(1 + \alpha_s^2 - 2\eta\alpha_s) \exp[2\varepsilon(\pi - \theta_l)]$$
$$\times \sin\left(\frac{3\theta_l}{2} - \phi - \varepsilon \ln r_l\right) - 2\varepsilon(1 + \alpha_s^2 + 2\eta\alpha_s) \sin\left(\frac{3\theta_l}{2} + \phi + \varepsilon \ln r_1\right)\Bigg] \tag{19}$$

where A is defined in eqn (18) and $0 \leq \theta \leq \pi$.

From the above discussion it becomes obvious that extraction of parameters is now possible provided that experimental data are gathered from a region near the moving crack tip characterized by the structure presented in eqns (18) and (19) (mixed-mode K^d-dominance).

Guided by the shape of the three-dimensional zone (see Figs 11 and 12) one expects that such a $|K^d|$-dominant region *may* exist for the wedge $100° < \theta < 150°$. Indeed, our numerical calculations show that the plane stress description is accurate in this wedge for $0{\cdot}1\,h < r < h$. For $r > h$, a higher-order plane stress expansion seems to be necessary. In addition and as will become obvious from the fringe patterns presented later, this region is characterized by a high density of CGS fringes. Use of eqn (19) in relations (5) for CGS allows for the estimation of the time variation of the parameters $|K^d(t)|$ and $\phi(t)$ during crack growth. This is done by fitting the experimental data (in regions of expected $|K^d|$-dominance) to the expected analytical form. This becomes possible provided that the crack-tip speed $v(t)$ is independently measured during the dynamic event. Finally, knowledge of $|K^d(t)|$ and $v(t)$ allows for the estimation of the dynamic energy release rate $G^d(v)$.

DYNAMIC EXPERIMENTS

Bimaterial specimen preparation

Bimaterial specimens used in the dynamic experiments are of the symmetric three-point bending configuration (Fig. 10). They are made from equal two thickness sheets (thickness $h = 9$ mm) of commercially available polymethyl methacrylate (PMMA) (material 1) and Al 6061-T6 or AISI-4340 (material 2). The two halves of the specimen are machined to ensure square edges and the bond face of aluminum or steel is sand-blasted using 10–20 μm glass beads. The bond between the two materials is created using a commercially available (see Tippur and

Rosakis[2]) methacrylate monomer (MMA) which polymerizes at ambient temperature when mixed with a catalyst. This results in a bond material with stiffness characteristics similar to that of material 1. The two-part compound is mixed in the ratio of 100 parts by weight of MMA monomer and 13 parts by weight of the catalyst. The aluminum or steel face of the bond is coated with a thin layer of the mixture and held against the PMMA with a uniform pressure. The bond is cured at ambient temperature for 48 h and the resulting thickness is approximately 100 μm. More details regarding the bonding procedure can be found in Tippur and Rosakis.[20]

Since it is essential to ensure that the stiffness characteristics of the bond material conform with that of PMMA and in order to describe the specimen as a *bimaterial* system, a quasistatic, bond-calibration test is performed. This test uses three-point bend specimens in which both halves (materials 1 and 2) of the specimen are made of equal thickness ($h = 9$ mm) PMMA sheets and are bonded together using the above prescribed procedure. The experimental results obtained from these specimens are compared with those of a *homogeneous* PMMA specimen (no bond) in the same three-point bending configuration, as described in detail by Tippur and Rosakis.[20]

The calibration tests reveal that cracks in the PMMA–PMMA bounded specimens have quasistatic toughnesses very close (up to 5%) of those of homogeneous PMMA. This testifies to the strength of the proposed bond and becomes important in the discussion of the dynamic results presented below.

Preliminary observations of dynamic crack growth, results and discussion

The bimaterial specimens used in the dynamic experiments have a 25-mm long pre-cut edge notch along the interface. After the initiation event, the crack propagates dynamically along the interface. The bimaterial specimens are impact-loaded in a drop-weight tower (Dynatup-8100A); see Fig. 10. Intense stress waves generated by the impact and reflected by the specimen boundaries load the notch tip up to crack initiation and the initiated crack propagates dynamically along the interfaces at speeds up to 800 m/s for the PMMA–Al bond and up to 950 m/s for the PMMA–steel bond. The transmission CGS technique is used in conjunction with high-speed photography to record dynamic crack-tip fields in a region approximately 50 mm in diameter around the notch tip. A rotating-mirror, high-speed camera (Cordin 330A) is used to photograph the fringes. Discrete images corresponding to different

stages of crack growth are formed by using a pulse laser as the light source. The light source is a Spectra-Physics Argon-Ion pulse laser (model 166). Short pulses of 20 ns duration produce sharp interference patterns during crack growth. The interval between successive light pulses is set as 1 μs (10^6 frames/s). The high-speed turbine is brought up to the required speed and the camera shutter is triggered open before the falling weight makes contact with the specimen. When the drop-weight contacts the specimen, the laser starts pulsing and the event is recorded on the film tract.

Unlike dynamic crack-growth experiments in homogeneous specimens, experiments conducted with bimaterial specimens pose an additional degree of complexity in conducting the tests. In reality, it is very difficult to impact the specimens exactly along the thin (100 μm) interface. Any slight experimental asymmetry results in an impact either side of the aluminum or steel half or the PMMA half of the specimen. Due to the differences in the wave-propagation speeds in the two materials, the dynamic loading histories of the crack tip corresponding to these situations differ vastly from one to the other. Thus, we had to choose to impact either the metal or the PMMA half of the specimen. In this preliminary report, we describe one set of results from dynamic experiments in which impact occurs on the metal half of the specimen at a small distance (5 mm) away from the interface. A typical sequence of crack-tip interference patterns ($\Delta = 44$ mm) of the field quantity $ch\,\partial(\hat{\sigma}_{11} + \hat{\sigma}_{22})/\partial x_1$ in PMMA is shown in Fig. 13. The bimaterial combination shown is PMMA–steel. The time $t = 0$ corresponds to crack initiation. At this point we refrain from reporting the complete time histories of G^d and ϕ during dynamic crack growth before a critical mass of experiments are analyzed and before definite statements regarding a dynamic crack-growth criterion can be made with confidence. However, we feel that we can report on our observations regarding the crack-tip velocity measured in the first set of experiments (six tests in PMMA/Al; six tests in PMMA–steel).

When the crack imitiates ($G \sim 150\,n/m$, $\phi \sim 50°$), intense stress waves emanate from the crack tip. These waves are visible in Fig. 13 as discrete kinds in otherwise smooth CGS fringes. This observation is a reliable sign of the existence of very strong dynamic effects and of high velocities of crack growth that are a large fraction of $c_R^{(1)}$ (the Rayleigh wave speed of PMMA). It should be noted that such waves are not usually visible after crack initiation in homogeneous PMMA specimens of the same configuration and loading where the observed *maximum* crack-tip speeds are $0{\cdot}35\,c_R$. However, such waves appear in optical CGS or caustic patterns of crack growth in high-strength materials (see

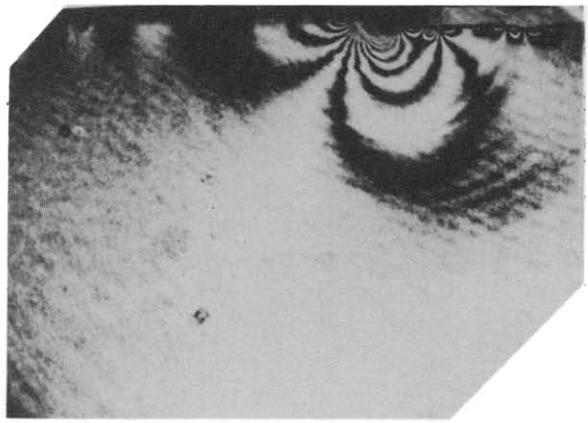

t=14 μs

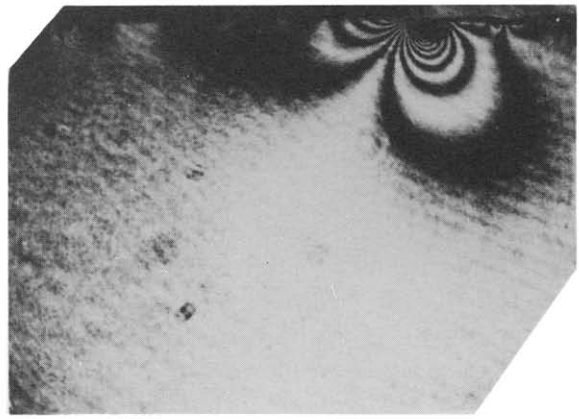

t=7 μs

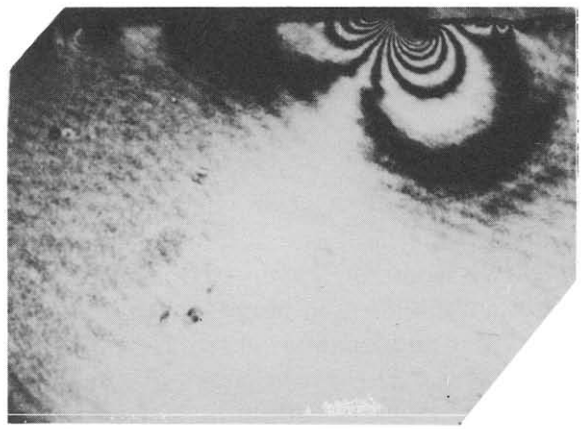

t=0 μs

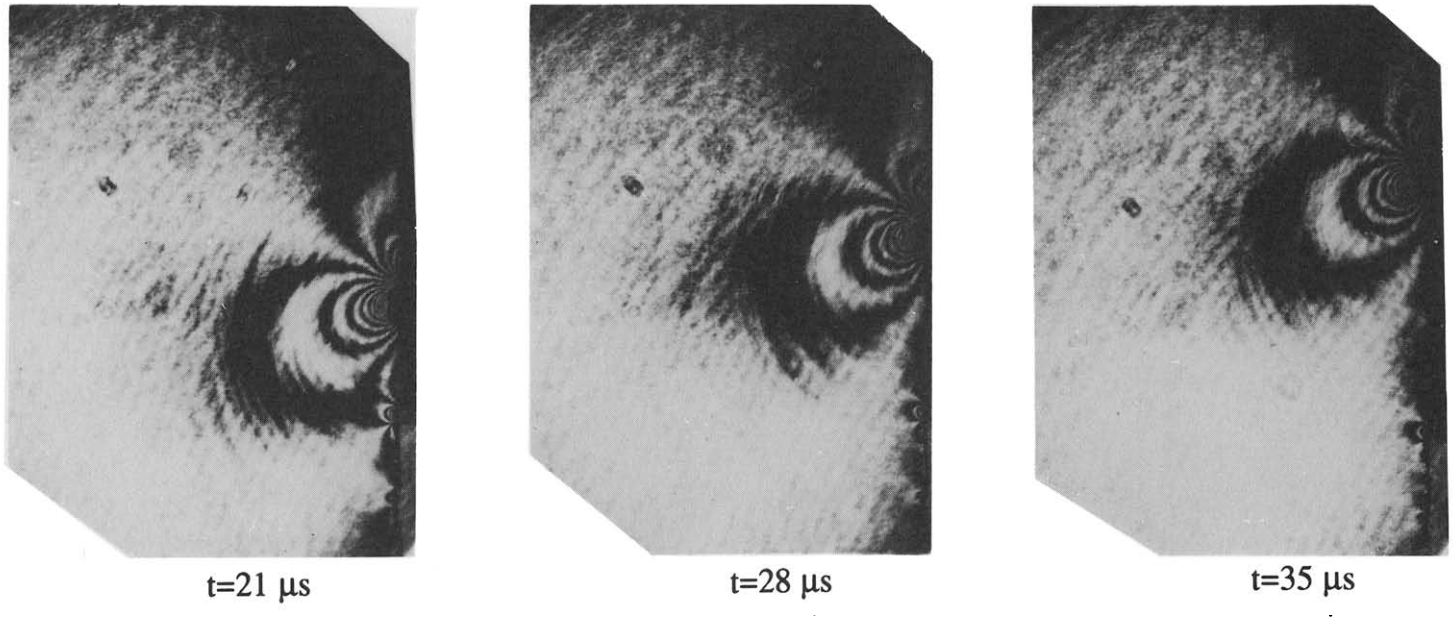

Fig. 13. CGS pattern of $\partial(\Delta S_1)/\partial x_1$ (PMMA side) near a dynamically initiating and growing crack along a PMMA–steel interface. The x_1-direction is the direction of the interface. (From Lambros and Rosakis[21].)

Rosakis[5]), when crack-tip velocities are in excess of $0{\cdot}4\,c_R$. (See also Fig. 9.)

A representative data set for the velocity and acceleration histories for a crack in a PMMA–steel specimen are shown in Fig. 14(a) and (b). Figure 14(a) reveals very high crack-growth velocities at times larger

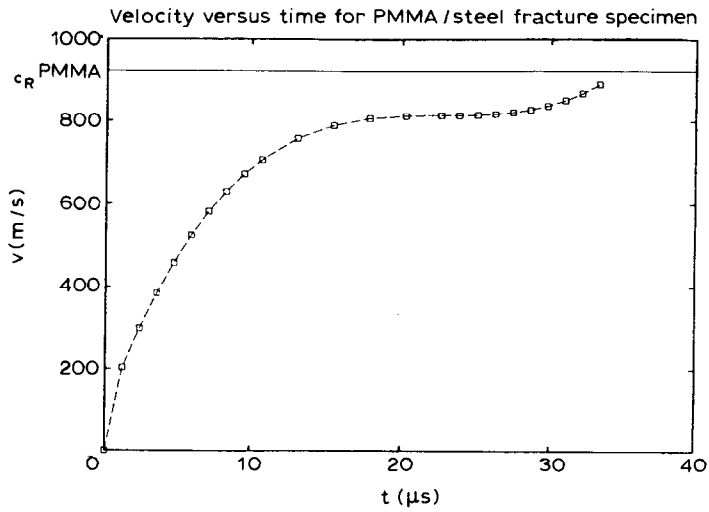

(a)

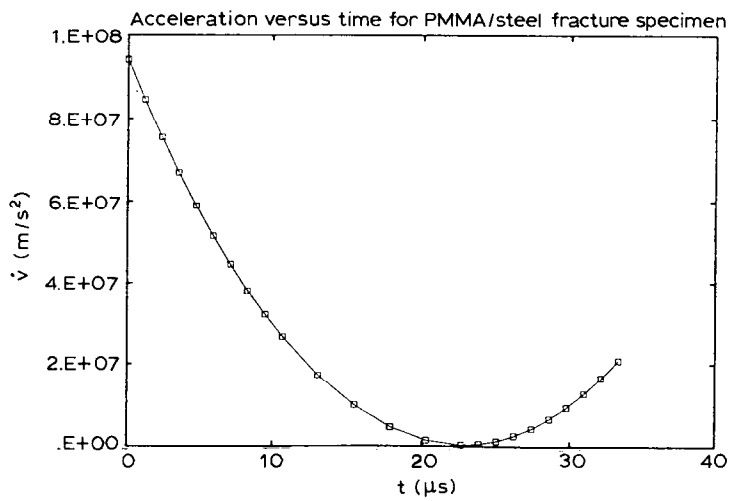

(b)

Fig. 14. Velocity and acceleration histories for the initial states of crack growth in a PMMA–steel interface. (From Lambros and Rosakis[21].)

than 20 μs after initiation. The maximum recorded velocity is approximately 95% of c_R^{PMMA} ($c_R^{PMMA} \sim 950$ m/s).

Crack-tip accelerations (shown in Fig. 14(b)) are also very high in the initial stages of crack growth (of the order of $10^6 g$, where g is the gravitational acceleration). The above observations are consistent with the visual evidence of the existence of intense stress waves emanating from the crack tip after the crack initiates.

The observation of very large crack-growth velocities was rather surprising given previous experience with dynamic crack growth in homogeneous PMMA specimens of the same configuration and loading (maximum speeds $\sim 0{\cdot}35\, c_R^{PMMA}$). Attributing such phenomenon to the existence of a weak bond is not very convincing since our bond-calibration technique revealed a bond-fracture toughness very close to that of PMMA. As a result we believe that the reason for such high speeds of propagation is intimately related to the strong material properties mismatch between PMMA and steel. This mismatch is expected to produce a complicated mechanism of energy storage in the Al side and subsequent energy transfer from the steel to the PMMA.

The observation of very high crack-tip acceleration indicates that transient effects may play a crucial role in the formation of the fringe patterns. Thus it is expected that in this case a transient higher-order expansion for the near-tip field for bimaterial cracks would need to be developed and applied to the analysis of the CGS patterns. The need for this step seems to be far more important than in the fracture of homogeneous solids.

Our experimental observation of high speeds of crack growth are corroborated by recent theoretical results by Yang *et al.*,[19] who studied dynamic crack growth along *perfectly bonded* bimaterial interfaces. One very important conclusion of this study is that as the crack-tip velocity approaches the lowest of the two Rayleigh wave speeds, say $c_R^{(1)}$, where $c_R^{(1)} < c_R^{(2)}$, a finite amount of energy has to be transmitted to the crack tip to maintain extension at $c_R^{(1)}$ if $|K^d|$ is non-zero. This is unlike the homogeneous case where an *infinite* amount of energy has to be transmitted to the crack tip to maintain extension at c_R if $|K^d|$ is non-zero. This obviously makes it energetically impossible for a crack, in a homogeneous solid, to exceed the material Rayleigh wave speed. Since no such energetic restriction exists for bimaterial systems and since the present experiments have already produced large propagation velocities, we intend to investigate the possibilities of bimaterial cracks propagating in the range $c_R^{(1)} < v < c_R^{(2)}$.

The experimental results reported here are very preliminary. We are currently in the process of developing a transient high-order expansion

for the dynamically growing crack in a bimaterial. This expansion will be used to analyze the dynamic optical CGS fringe patterns so that definite statements can be made regarding the velocity dependence of fracture toughness and mode mixity.

ACKNOWLEDGEMENTS

The support of ONR Contract N000 14-90-J-1340 and NSF Grant No. MSS-9024838 is gratefully acknowledged. The author would also like to acknowledge the contributions of his past and present collaborators —Professors L. B. Freund of Brown University, S. Krishnaswamy of Northwestern University, H. V. Tippur of the University of Aubory and Dr Y. J. Lee of Dow Chemical.

REFERENCES

1. Tippur, H. V., Krishnaswamy, S. & Rosakis, A. J., A coherent gradient sensor for crack tip deformation measurements: analysis and experimental results. *Int. J. Fracture,* **48** (1991) 193–204.
2. Tippur, H. V., Krishnaswamy, S. & Rosakis, A. J., Optical mapping of crack tip deformations using the method of transmission and reflection coherent gradient sensing: a study of crack-tip K-dominance. Caltech Report SM89-11, (1989); *Int. J. Fracture,* **52** (1991) 91–117.
3. Sanford, R. J. & Dally, J. W., A general method for determining mixed-mode stress intensity factors from isochromatic fringe patterns. *Eng. Fract. Mech.,* **11** (1979), 621–33.
4. Burger, C. P., Photoelasticity. In *Handbook on Experimental Mechanics,* ed. A. S. Kobayashi, 1987, pp. 162–281.
5. Rosakis, A. J., Two optical techniques sensitive to gradients of optical path difference: the method of caustics and the coherent gradient sensor (CGS). In *Experimental Techniques in Fracture,* Vol. III ed. J. Epstein, 1993.
6. Chiang, F. P. & Hareesh, T. V. Three-dimensional crack tip deformation: an experimental study and comparison to HRR field. *Int. J. Fract.,* **36** (1988) 243–57.
7. Kang, B. S. J., Kobayashi, A. S. & Post, D., Stable crack growth in aluminum tensile specimens. *Exper. Mech.,* **27**(3) (1987) 243–5.
8. Krishnaswamy, S., Tippur, H. V. & Rosakis, A. J., Measurement of transient crack tip deformation fields using the method of coherent gradient sensing. California Institue of Technology GALCIT Report SM 90-1; *J. Mech. Phys. of Solids,* **40**(2) (1992) 1–24.
9. Freund, L. B. & Rosakis, A. J., The influence of transient effects on the asymptotic crack tip field during dynamic crack growth. 11*th National Congress of Applied Mechanics, Tucson, Arizona, May* 1990; *J. Mech. Phys. Solids,* **40**(3) (1992) 699–719.

10. Rosakis, A. J., Liu, C. & Freund, L. B., A note on the asymptotic stress field of a non-uniformly propagating dynamic crack. California Institute of Technology GALCIT Report SM 90-27; *Int. J. Fract.,* **50** (1991) R39–R45.
11. Rosakis, A. J. & Ravi-Chandar, K., On the crack tip stress state: an experimental evaluation of three-dimensional effects. *Int. J. Solids Structures,* **22**(2) (1986) 121–34.
12. Liu, C., Rosakis, A. J. & Freund, L. B., The interpretation of optical caustics in the presence of non-uniform crack to tip motion histories: a study based on a higher order transient crack tip expansion. *J. Solids Structures* (in press).
13. Kahthoff, J. F., Shadow optical method of caustic. In *Handbook of Experimental Mechanics,* ed. A. S. Kobayashi. (1987), pp. 430–98.
14. Rosakis, A. J., Duffy, J. & Freund, L. B., The determination of the dynamic fracture toughness of AISI 4340 steel by the shadow spot method. *J. Mech. Phys. Solids,* **34**(4) (1984) 443–60.
15. Freund, L. B., *Dynamic Fracture Mechanics.* Cambridge University Press, Cambridge, 1990.
16. Krishnaswamy, S. & Rosakis, A. J., On the extent of dominance of asymptotic elastodynamic crack tip fields; part I: an experimental study using bifocal caustics. *J. Appl. Mech.* **57**(1) (1991) 87–94.
17. Dally, J. W., Fourney, W. G. & Irwin, G. R., On the uniqueness of K_{ID}–$\dot{a}$ relation. *Int. J. Fract.,* **27** (1985) 159–68.
18. Lee, Y. J. & Roskis, A. J., Interfacial cracks in plates: part I. three-dimensional numerical investigation. *Inter. J. Solids Structures* (in press).
19. Yang, W., Suo, Z. and Shih, C. F., Mechanics of Dynamic debonding. *Proc. Royal Soc. London,* **A433** (1991) 679–97.
20. Tippur, H. V. & Rosakis, A. J. Quasitatatic and dynamic crack growth along bimaterial interfaces; a note on crack tip field measurements using coherent gradient sensing. *J. Expl Mech.,* **31** (1991) 243–51.
21. Lambros, J. Rosakis, A. J., work in progress (1993).